Åbo Akademi

Jani Trygg

Functional Cellulose Microspheres For Pharmaceutical Applications

Laboratory of Fibre and Cellulose Technology
Faculty of Science and Engineering
Åbo Akademi University

Turku / Åbo 2015

"Education is what survives
when what has been learned
has been forgotten."
-B.F. Skinner

Jani Trygg

Born 1981, Turku, Finland.

He received M.Sc. in chemistry from University of Turku in 2008, started Ph.D. studies at Laboratory of Fibre and Cellulose Technology in Åbo Akademi in 2009 and had his Ph.D. dissertation in Åbo Akademi in 2015.

Åbo Akademis förlag
Tavastgatan 13, FI-20500 Åbo, Finland
Tfn +358 (0)2 215 3478
E-post: forlaget@abo.fi

Försäljning och distribution:
Åbo Akademis bibliotek
Domkyrkogatan 2–4, FI-20500 Åbo, Finland
Tfn +358 (0)2 -215 4190
E-post: publikationer@abo.fi

Functional Cellulose Microspheres For Pharmaceutical Applications

Jani Trygg

Laboratory of Fibre and Cellulose Technology
Faculty of Science and Engineering
Åbo Akademi University

Turku / Åbo 2015

Supervisor
Professor Pedro Fardim
Laboratory of Fibre and Cellulose Technology
Faculty of Science and Engineering
Åbo Akademi University, Finland

Opponent
Professor Patrick Navard
Ecole des Mines de Paris / CEMEF, France

Reviewers
Professor Patrick Navard
Ecole des Mines de Paris / CEMEF, France

Professor Ilkka Kilpeläinen
Laboratory of Organic Chemistry
Department of Chemistry, Faculty of Science
University of Helsinki, Finland

ISBN 978-952-12-3168-1
Suomen Yliopistopaino Oy, Juvenes Print, Turku 2015

Abstract

Jani Trygg

Functional Cellulose Microspheres for Pharmaceutical Applications

Doctor of Philosophy in Chemical Engineering Thesis

Åbo Akademi University, Faculty of Science and Engineering,
Laboratory of Fibre and Cellulose Technology, Turku 2015.

Keywords: Cellulose, pretreatment, viscosity, degree of polymerisation, dissolution, coagulation, regeneration, microsphere, bead, surface area, porosity, functionalisation, oxidation, drug delivery, release profile

Dissolving cellulose is the first main step in preparing novel cellulosic materials. Since cellulosic fibres cannot be easily dissolved in water-based solvents, fibres were pretreated with ethanol-acid solution prior to the dissolution. Solubility and changes on the surface of the fibres were studied with microscopy and capillary viscometry. After the treatment, the cellulose fibres were soluble in alkaline urea-water solvent. The nature of this viscous solution was studied rheologically.

Cellulose microspheres were prepared by extruding the alkaline cellulose solution through the needle into an acidic medium. By altering the temperature and acidity of the medium it was possible to adjust the specific surface area and pore sizes of the microspheres. A typical skin-core structure was found in all samples.

Microspheres were oxidised in order to introduce anionic carboxylic acid groups (AGs). Anionic microspheres are more hydrophilic; their water-uptake increased 25 times after oxidation and they could swell almost to their original state (88%) after drying and shrinking. Swelling was studied in simulated physiological environments, corresponding to stomach acid and intestines (pH 1.2-7.4).

Oxidised microspheres were used as a drug carriers. They demonstrated a high mass uniformity, which would enable their use for personalised dosing among different patients, including children. The drug was solidified in microspheres in amorphous form. This enhanced solubility and could be used for more challenging drugs with poor solubility. The pores of the microspheres also remained open after the drug was loaded and they were dried. Regardless of the swelling, the drug was released at a constant rate in all environments.

Tiivistelmä

Jani Trygg:
Functional Cellulose Microspheres for Pharmaceutical Applications
(Muokatut selluloosahelmet farmaseuttisissa sovelluksissa)
Väitöskirja
Åbo Akademi, Luonnontieteiden ja tekniikan tiedekunta,
Kuitu- ja selluloosateknologian laboratorio, Turku 2015.
Avainsanat: Selluloosa, esikäsittely, viskositeetti, polymerisaatioaste, liuotus, koagulointi, regenerointi, helmi, pinta-ala, huokoisuus, muokkaus, hapetus, lääkeannostelu, vapautumisprofiili

Selluloosan liuotus on ensiaskel valmistettaessa uusia selluloosamateriaaleja. Koska selluloosakuituja ei voi helposti liuottaa vesi-pohjaisiin liuottimiin, kuidut esikäsiteltiin etanoli-hapolla ennen liuotusta. Muutoksia kuitujen pintarakenteessa ja liukoisuudessa tutkittiin mikroskoopeilla ja kapillaariviskometrilla. Käsittelyn jälkeen kuidut liukenivat emäksiseen urean vesiliuokseen. Tämän liuoksen luonnetta tutkittiin reologisesti.
Selluloosahelmet valmistettiin pursuttamalla alkaalinen liuos pisaroittain neulan läpi happamaan vesiliuokseen. Muuttamalla vesiliuoksen lämpötilaa ja happamuutta voitiin säädellä helmien ominaispinta-alaa ja huokosia. Tyypillinen kuori-ydin -rakenne löydettiin kaikista näytteistä.
Helmiin lisättiin anionisia karboksyylihappo-ryhmiä hapettamalla. Anioniset helmet olivat enemmän hydrofiilisiä; niiden vedenottokyky kasvoi 25 kertaiseksi hapetuksen jälkeen ja ne turposivat lähes alkuperäisiin mittoihin (88%) kuivauksen aikana tapahtuneen kutistumisen jälkeen. Turpoamista tutkittiin keinotekoisissa fysiologisissa ympäristöissä, jotka vastasivat vatsahappoa ja suolistoa (pH 1,2-7,4).
Hapetettuja selluloosahelmiä käytettiin lääkkeenkantajina. Ne osoittivat erittäin tasaista massajakaumaa, jota voitaisiin hyödyntää esimerkiksi henkilökohtaisessa lääkkeenannostelussa vaikka lapsipotilailla. Lääke oli kuivunut kidemuodottomaksi helmen huokosiin, joka osaltaan edisti vapautumista. Tätä voitaisin käyttää heikkoliukoisten lääkeaineiden kuljettamisessa elimistöön. Huokoset pysyivät auki kun lääkkeillä ladatut helmet kuivattiin. Huolimatta turpoamisnopeudesta, lääkeaine vapautui vakionopeudella jokaisessa tutkitussa ympäristössä avonaisten huokosten ansiosta.

Sammanfattning

Jani Trygg: Functional Cellulose Microspheres for Pharmaceutical Applications (Funktionella cellulosapärlor för farmaceutiska tillämpningar)
Avhandling
Åbo Akademi, Fakulteten för naturvetenskaper och teknik,
Laboratoriet för fiber- och cellulosateknologi, Åbo 2015.
Nyckelord: Cellulosa, förbehandling, viskositet, polymerisationsgrad, upplösning, koagulering, regenerering, cellulosapärla, ytarea, porositet, funktionalisering, oxidering, läkemedelsdosering, profil av läkemedelsfrisättning

Upplösning av cellulosa är det första steget vid framställning av nya cellulosamaterial. Eftersom cellulosabaserade fibrer inte kan lätt upplösas i vattenbaserade lösningsmedel, gjordes en förbehandling av fibrerna med en etanolsyralösning före själva upplösningen. Förändringar i fibrernas ytstruktur och upplösningsegenskaper studerades med mikroskop och kapillärviskometri. Efter förbehandlingen löste sig fibrerna i alkalisk urea-vatten lösning. Denna cellulosalösnings egenskaper karakteriserades reologiskt.
Cellulosapärlor framställdes genom att extrudera den alkaliska cellulosalösningen genom en nål till en sur vattenlösning. Genom att ändra vattenlösningens temperatur och surhetsgrad var det möjligt att skräddarsy cellulosapärlornas specifika ytarea och porstorlek. Alla prov visade sig ha en typisk skinn-kärna struktur.
Cellulosapärlorna oxiderades för att införa anjoniska karboxylsyragrupper. De anjoniska cellulosapärlorna visade en större hydrofilisitet; deras vattenupptagningsförmåga ökade 25-falt efter oxideringen och de kunde nästan svälla tillbaka till sin ursprungliga storlek (88%) efter föregående torkning och krympning. Svällningen undersöktes i simulerade fysiologiska miljöer, vilka motsvarade magsyra och tarmar (pH 1,2-7,4).
Oxiderade cellulosapärlor användes som läkemedelsbärare. De visade sig ha en väldigt jämn massafördelning, vilket kunde utnyttjas till personliga läkemedelsdoseringar för olika patienter, exempelvis till barn. Medicinen var solidifierad inne i cellulosapärlorna i en amorf form, vilket delvis gynnade läkemedlets frigivning och löslighet. Detta kunde användas till att transportera svårlösliga läkemedel till kroppen. Cellulosapärlornas porer förblev öppna efter att pärlorna fyllts med läkemedel och torkats. Oberoende av svällningshastigheten frigjordes läkemedlet med en konstant hastighet i alla de studerade miljöerna tack vare de öppna porerna.

Contents

List of Figures

List of Tables

Nomenclature

Symbols

λ	Wavelength
c	Concentration
G' and G"	Storage and loss moduli
k	Release constant
m	Mass
M_t and M_∞	Measured amount of drug at time t and infinite time.
P	Power
pK_a	Acid dissociation constant
T	Temperature
t	Time
tanα	Angle of repose
V	Volume

Units

ν	Frequency of the wave
°	Degree
°C	Celsius degree
Å	Ångström, 10^{-10}m
cm^3	Cubic centimetre
cm^{-1}	Wavenumber
dm^3	Cubic decimetre

G	Standard gravity
g	Gram
g cm^{-3}	Gram per cubic centimetre
h	Hour
K	Kelvin
M	Molar, mol dm^{-3}
m	Metre
m^2g^{-1}	Square metre per gram
min	Minute
mol	Mole, ~6.022×10^{23}
s^{-1}	Reciprocal seconds
V	Volt
W	Watt

Abbreviations and acronyms

-COOH	Carboxylic acid group
μ_	Micro-, 10^{-6}
ACB	Anionic cellulose bead
AG	Anionic group
AGU	Anhydroglucose unit
API	Active pharmaceutical ingredient
BMIMAc	1-butyl-3-methylimidazolium acetate
BMIMCl	1-butyl-3-methylimidazolium chloride
CaF_2	Calcium fluoride
CED	Cupriethylene diamine

CMC	Carboxymethyl cellulose
CO_2	Carbon dioxide
CPD	Critical point dried
CS_2	Carbon disulphide
DIN	German Institute for Standardisation
DLaTGS-KBr	Deuterated L-alanine doped triglycine sulphate-potassium bromide
DMAc/LiCl	N,N-dimethylacetamide with lithium chloride
DMS	Trans-4-[4-(Dimethyl-amino)styryl]-1-methylpyridinium iodide
DP_v	Viscosity average degree of polymerisation
DS	Degree of substitution
DSC	Differential scanning calorimeter
E_a	Apparent activation energy
EC	Ethyl cellulose
EHS	Environmental, health and safety requirements
FTIR	Fourier transform infrared spectrometer
HEMA	Poly(hydroxyethyl methacrylate)
HNO_3	Nitric acid
HPC	Hydroxypropyl cellulose
HPMC	Hydroxypropyl methylcellulose
ILs	Ionic liquids
InGaAs	Indium gallium arsenide
ISO/FDIS	International Organisation for Standardisation / Final Draft International Standard

k_	Kilo-, $\times 10^3$
M_	Mega-, $\times 10^6$
m_	Milli-, $\times 10^{-3}$
MC	Methyl cellulose
MEC	Methylethyl cellulose
n_	Nano-, $\times 10^{-9}$
Na	Sodium
NaCl	Sodium chloride
NaClO	Sodium hypochlorite
$NaClO_2$	Sodium chlorite
NaH_2PO_4	Sodium dihydrogen phosphate
NaOH	Sodium hydroxide
NMMO	N-methylmorpholine N-monohydrate
OCB	Oxidised cellulose bead
P- and S1,2-layer	Primary and secondary layers of the fibre
PEG	Polyethylene glycol
pH	Potential of hydrogen, acidity
PVA	Poly(vinyl alcohol)
R^2	The coefficient of determination
R-	Cellulose backbone
Ran.HCl	Ranitidine hydrochloride
SAXS	Small angle X-ray scattering
SCAN-Test	Scandinavian Pulp, Paper and Board Testing Committee
SEC	Size-exclusion chromatography

SSA	Specific surface area
TEMPO	(2,2,6,6-tetramethylpiperidin-1-yl)oxidanyl
ToF-SIMS	Time of flight secondary ion mass spectrometry
USP-NF	United States Pharmacopeia - The National Formulary

Preface

This thesis is based on work done at the Laboratory of Fibre and Cellulose Technology between 2009 and 2014 under the supervision of Professor Pedro Fardim. The results are published in peer-reviewed scientific journals and are referred to in the text as Papers I-V. Additionally three supporting publications (1-3) are used in context.

Paper I	Trygg, J. & Fardim, P., Enhancement of cellulose dissolution in water-based solvent via ethanol-hydrochloric acid pretreatment, *Cellulose* **18** (2011) 987-994.
Paper II	Trygg, J.; Fardim, P.; Gericke, Mäkilä, E. & Salonen, J., Physicochemical design of the morphology and ultrastructure of cellulose beads, *Carbohydrate Polymers* **1** (2013) 291-299.
Paper III	Trygg, J.; Yildir, E.; Kolakovic, R.; Sandler, N. & Fardim, P., Anionic cellulose beads for drug encapsulation and release, *Cellulose* **21** (2014) 1945-1955.
Paper IV	Trygg, J.; Yildir, E.; Kolakovic, R.; Sandler, N. & Fardim, P., Solid-state properties and controlled release of ranitidine hydrochloride from tailored oxidised cellulose beads, *Macromolecular Materials and Engineering* (2014) DOI 10.1002/mame.201400175.
Paper V	Gericke, M.; Trygg, J. & Fardim, P., Functional cellulose microspheres - Preparation, characterization, and applications. *Chemical Reviews* **113** (2013) 4812-4836.

Supporting publications

1 Trygg, J.; Gericke, M. & Fardim, P., Chapter 10. Functional Cellulose Microspheres. In Valentin Popa (editor), *Pulp Production and Processing: From Papermaking to High-Tech Products*. Smithers Rapra Technology, Shawburry, Shrewsbury, Shropshire, UK, 2013.

2 Trygg, J.; Gericke, M. & Fardim, P., Functional cellulose spheres for advanced applications, *The 9th Biennial Johan Gullichsen Colloquium*, Proceedings, 2013.

3 Yildir, E.; Kolakovic, R.; Genina, N.; Trygg, J.; Gericke, M.; Hanski, L.; Ehlers, H.; Rantanen, J.; Tenho, M.; Vuorela, P.; Fardim, P. & Sandler, N., Tailored beads made of dissolved cellulose - investigation of their drug release properties. *International Journal of Pharmaceutics* **18** (2013) 417-423.

Author's contribution

I All experiments excluding FE-SEM. Interpretation of the results and writing the manuscript.

II All experiments excluding FE-SEM and nitrogen adsorption. Interpretation of the results and writing the manuscript.

III All experiments excluding FE-SEM and drug release measurements. Interpretation of the results and writing the manuscript.

IV All experiments excluding drug release measurements. Interpretation of the results and writing the manuscript.

V Co-author.

1 Writing author.

2 Writing author.

3 Co-author.

1 Introduction

Novel cellulosic shapes have gained increasing interest among researchers, partly due to global trends to utilise renewable materials in areas which had formerly used, for example, oil-based products. Another motivation includes new markets and products which had not existed before but for which there is a niche. In either case the preparation of an adaptable product requires preliminary research at each phase of the product development.

Forming new shapes from cellulose requires the destruction of the intermolecular network of the cellulose molecules. Dissolving cellulose either directly or after chemical modification destroys the hydrogen bonds and separates the molecules from each other, making it possible to "build up" new shapes at this level. Conventionally, cellulose has been dissolved using toxic materials such as metal complexes or viscose process, but in the 1990's novel water-based solvents started to gain more attention due to environmental regulations and academic research (Isogai and Atalla, 1998; Kamide et al., 1992). At the beginning of the 2000s ionic liquids became more interesting due to their ability to dissolve high amounts of cellulose (Swatloski et al., 2002). However, the choice of the solvent is mainly influenced by the need for and possibilities in a process, and of course the properties desired from the end product.

A new shape is formed by shaping the cellulose dope and either hindering the effectiveness of the solvent, neutralising it, or converting soluble cellulose derivatives back to insoluble cellulose. The shape itself can be considered a functional property if it can be adjusted and utilised in an application.

Another possibility is to modify cellulose chemically by derivatisation, either hetero- or homogeneously. Since the application defines the properties that are required from the material, it is necessary to acknowledge these properties at the very beginning of the process, for example short-chained cellulose should be avoided if pulling a yarn for high-tensile strength applications (Krässig and Kitchen, 1961; Woodings, C. and Textile Institute (Manchester, England), 2001).

Different cellulosic shapes can be placed in two categories; native and ar-

tificial (Figure 1.1). The properties of the material in both categories are connected to the geometric form of the product and cellulose as a structural polymer. In native shapes cellulose molecules are produced by biosynthesis; a polymerisation of the glucose units to cellulose. The shape of the product, starting from the orientation, packing, and length of the molecules, is determined by the biological needs. The most common native cellulosic shape is that of a plant fibre. It commonly consists of three layers, that is the primary, secondary and tertiary cell wall layers (Jensen, 1977) and can thus be considered to have a non-uniform morphology. Bacterial cellulose consists of microfibrils like plant fibres, but fibrils are ribbon-like, much smaller and initially more pure (Jonas and Farah, 1998).

Artificial cellulosic shapes are commonly formed via *gelation* of existing cellulose molecules. Gelation is usually undertaken by slowly forming the hydrogen bond network so that the newly formed network covers the whole space together with the liquid phase. This allows cellulose molecules to maximise their space and surface area (Gavillon and Budtova, 2008). The liquid can then be removed, for example by freeze-drying or critical point drying, to avoid hornification and to maintain the morphology. Since these products are often highly porous, they can be used, for instance, as an insulator. When the targeted property is liquid adsorption, they are commonly referred to as sponges. Additionally, cellulose is biocompatible (Miyamoto et al., 1989) and can be used in wound dressings (scaffolds) or in drug delivery. Sometimes they are called with prefix *aero-*, such as aerocellulose.

If the gelated shape is a spherical particle, it is commonly called a cellulose bead or microsphere. They have a diameter greater than 10 μm, separating them from nanomaterials, and cellulose is the main component giving the structural properties (Gericke et al., 2013). Otherwise the attributes are mainly the same as described above; high surface area, porosity, biocompatibility, and so on. Their sphericity and dimensions can also be utilised in applications, using, for example, their ability to flow.

The literature review of this doctoral thesis begins with an overview of cellulose structure and sources. Different pretreatments are presented prior to the dissolution of cellulosic fibres. The phenomena of regeneration and coagulation is clarified in the context of the different solvent systems. The section about controlled release systems leads the thesis to the challenges of designing polymer matrices for drug delivery. Essential characterisation methods

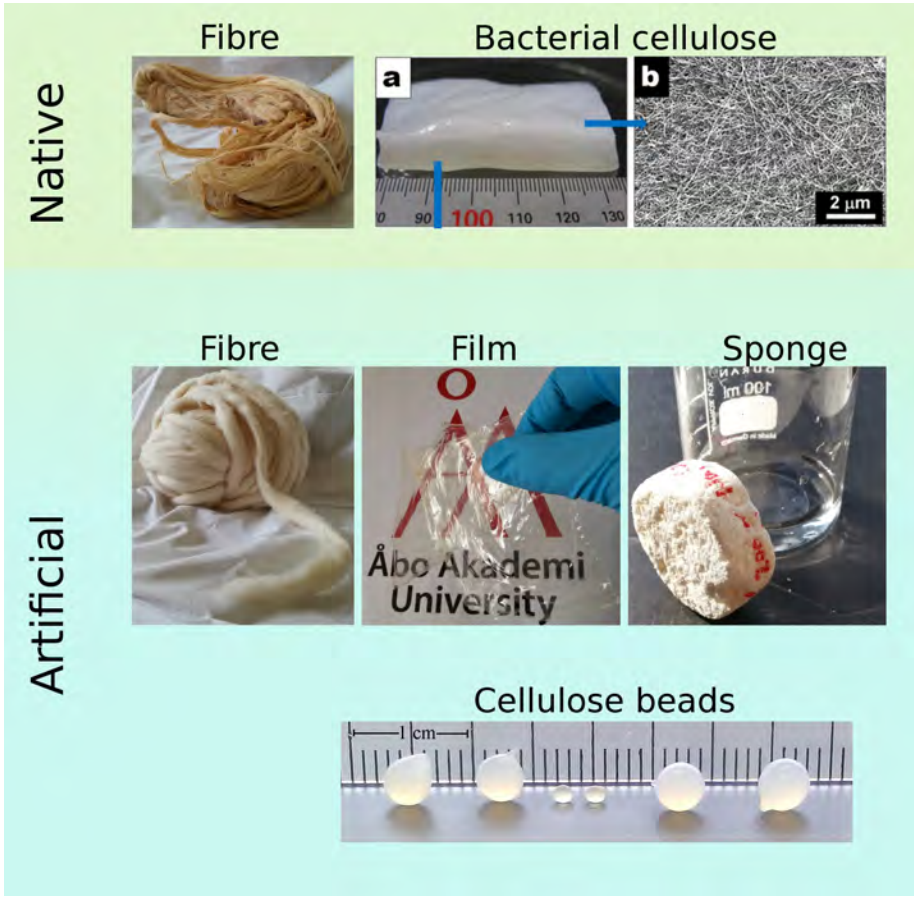

Figure 1.1: Cellulosic shapes. (Top) Native jute fibres and bacterial cellulose (photograph and SEM image), (bottom) regenerated cellulose fibres and films from viscose, and coagulated sponge and beads from NaOH/urea/water. Image of bacterial cellulose from Chen et al. (2010) and of beads from Trygg et al. (2014).

for cellulosic shapes and pharmaceutical applications are introduced at the end of the literature section of the thesis.

In the experimental section a complete preparation route is presented for functional cellulose microspheres. It presents the challenges to dissolving cellulose in water-based solvents and proposes an efficient pretreatment method to enhance solubility (Paper I). The physicochemical modification of microspheres is studied in order to understand the role of the coagulation environment and its utilisation for the final product (Paper II). This study was further expanded to be a complete study of drug delivery (Supporting Publication 3). Microspheres were chemically modified, their properties were characterised (Paper III) and their use in drug delivery was studied in detail (Paper IV). A review (Paper V) of potential applications is given in the end of the experimental section, based on the results presented in earlier papers and on observations during the studies.

1.1 Cellulose sources and structures

Approximately 1.5×10^{12} tons of cellulose biomass is produced on Earth each year (Klemm et al., 2005). Biosynthesis routes to cellulose formation are found in prokaryotes (Ross et al., 1991; Zogaj et al., 2001) and eukaryotes, such as animals (tunicates), various algae, fungi, and plants (Brown, 1985). Among cellulose producing bacteria, cyanobacteria has existed for more than 2.8 billion years (Nobles et al., 2001). Endosymbiotic transfer of the cellulose synthases has been proposed as occurring from cyanobacteria to plants. Speculation about the early purpose of cellulose vary from high UV radiation shielding of the early Earth to enhanced motility in organisms. As far as we know, nowadays cellulose mostly acts as a structural polymer providing strength and support for plants.

Cellulose is composed of 1→4 linked β-D-glucose units, each unit rotated 180° compared to the previous unit. It is a linear polymer which forms strong hydrogen bonding network via three hydroxyl groups (-OH) on its C2, C3 and C6 carbons. The orientation of these hydroxyl groups and the placement of the cellulose chains compared to neighbouring chains defines the crystal structure (allomorph) of the cellulose (Figure 1.2). Cellulose I is the most common allomorph with two suballomorphic forms, triclinic Iα and monoclinic Iβ unit cells (Zugenmaier, 2001). The former is mainly produced by algea and

bacteria and the latter by plants. Since the main source of artificial cellulosic products is dissolving pulp, which is made from wood biomass, cellulose Iβ is most used cellulose suballomorph. In this thesis, terms “cellulosic pulp”, “cellulosic fibre”, and “cellulose” exclusively refer to a material which is extracted from wood biomass.

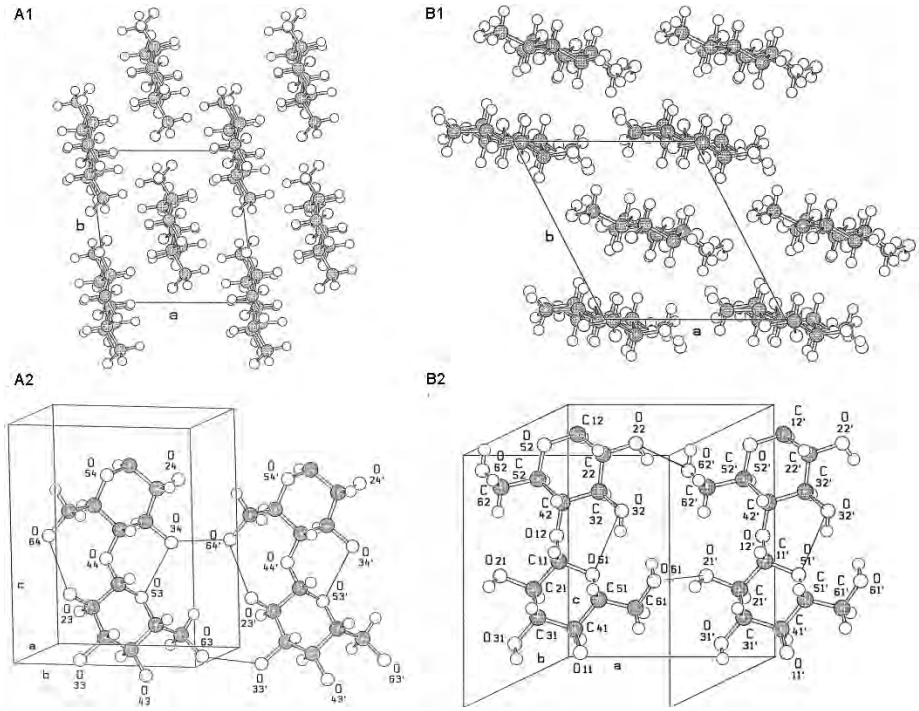

Figure 1.2: Representation of (A) cellulose Iβ and (B) cellulose II crystal structures on (A1,B1) **a-b** plane and (A2, B2) molecules in lattice planes 100 and 010, respectively. Figure from Zugenmaier (2001).

Both suballomorphs are described as thermodynamically less stable than cellulose II. Paradoxically, cellulose I is clearly more common in nature (so-called *native cellulose*) and cellulose II is seldom produced in small quantities, such as by Acetobacter Xylinum (Roberts et al., 1989). Cellulose II (generally in the literature as *regenerated cellulose*) is often produced from cellulose I by mercerization (treatment with aqueous sodium hydroxide) or after dissolution and coagulation. Other crystal structures, such as cellulose III and IV with their suballomorphs are even more rare in nature (Brown Jr et al., 1996), but can be artificially converted to cellulose III by ammonia treatment, and further to cellulose IV by heat treatment in glycerol (Zugenmaier, 2001).

1.2 Pretreatment of cellulosic pulp prior to dissolution

Cellulose is insoluble in most common solvents due to a strong inter- and intramolecular hydrogen bonding network (Klemm et al., 1998). If the cellulose molecules are long, the network is more dense and the solubility lower (Qi et al., 2008). Evolution has also developed wood fibres to be resistant against physical and chemical impacts, yielding fibres with three layers that provide resistivity against physical stress (Niklas, 1992) and its own chemical toxins in order to protect it from microorganisms and chemical attacks (Scheffer, 1966).

Pretreatments aim to break the original shape and/or composition of a pulp fibre (Mosier et al., 2005). Unwanted components in cellulosic pulp, such as hemicelluloses and lignin, can interfere with the dissolution process or chemical modification. The accessibility of the reagents into the fibre in both cases is essential for the successful processing and even distribution of the functional groups (Moigne et al., 2010).

Pretreatments can be roughly categorised into three classes: physical, chemical, and biological (Table 1.1). In physical methods, such as ball milling, mechanical energy is used to reduce the crystallinity and open the fibre (Tassinari et al., 1980). These are often very energy demanding methods, however (Kumar et al., 2009). Physicochemical methods, such as steam explosion and hot water treatment, are more cost effective (McMillan, 1994; Weil et al., 1997). They degrade hemicelluloses and disrupt lignin structures. As a downside, their byproducts might inhibit biological methods which are often used in biomass conversions (Palmqvist and Hahn-Hägerdal, 2000). Ammonia and CO_2 fibre explosions do not produce these inhibitory byproducts and they do open the fibre, but they are not effective against lignin and hemicelluloses (Kumar et al., 2009). Due to their low cost they are used as a preliminary method before enzymatic treatment (Yang and Wyman, 2006).

Biological (enzymatic) methods are targeted against certain components. Enzymes from biological origins are usually pH and temperature sensitive and other components may interfere with efficiency (Schilling et al., 2009). Chemical methods on the other hand are less specific but they are more available and more versatile (Adel et al., 2010; Kumar et al., 2009; Mosier et al., 2005). From a dissolution point of view, both methods, biological and chemical, aim at degradation of cellulose molecules to enhance solubility.

Table 1.1: Rough classes of the pretreatment methods of the biomass and their effects.

Class	Example method	Description	Ref #
Physical	Refining	Fibrillates and reduces crystallinity.	1
	Milling	Reduces crystallinity.	2
Physico-chemical	Heating	Solubilisation of hemicelluloses and partially lignin.	3
	Liquid hot water	Like heating but more effective.	4
	Steam explosion	Rapid depressurisation of water opens the fibre.	5
Chemical	Ozonolysis	Selective degradation of lignin, no effect on cellulose or hemicellulose.	6
	Acid hydrolysis	Hydrolyses hemicelluloses and cellulose.	7
	Alkaline hydrolysis	Removes hemicelluloses and swells the fibre.	8
	Oxidative delignification	Like alkaline hydrolysis with oxidative component. Lignin degradation.	9
	Organosolv	Acid hydrolysis in organic solvent.	10
Biological	Enzymatic	Yeast, fungi, moulds and bacteria based enzymes. Specific targets.	11

References: 1.Jonoobi et al. (2009), 2.Tassinari et al. (1980), 3.Hendriks and Zeeman (2009); Mosier et al. (2005), 4.Weil et al. (1997), 5.Li et al. (2009), 6.Quesada et al. (1999), 7.Lu et al. (2007), 8.Carrillo et al. (2005), 9.Kim and Holtzapple (2006), 10.Kumar et al. (2009), 11.Schilling et al. (2009).

1.3 Cellulose dissolution, regeneration, and coagulation

In order to dissolve cellulosic fibres, the solvent should penetrate the cell wall layers and disrupt the hydrogen bonding network to such an extent that cellulose molecules (and other components) no longer interact with each other. The affinity to the solvent has to be stronger than that which the dissolving components have for each other. If the solvent is efficient enough, dissolution proceeds via the fragmenting mechanism directly destroying all the layers of the fibre when in contact. This is usually the case with, for example, metal complexes and ionic liquids. Weaker solvents usually dissolve chemically less resistant layers first, the secondary and tertiary cell walls,

while the more resistant primary cell wall remains intact. This causes osmotic pressure inside the fibre, which can be seen as a “ballooning” phenomenon. This mechanism usually leaves undissolved fragments in the solution, as so-called ’collars’ between the balloons (Cuissinat and Navard, 2006a,b, 2008).

The hydrogen bonding network can be disrupted in two ways. In direct dissolution the network is broken by the presence of disruptors, electron donors and acceptors, and complexing molecules (Figure 1.3, right-side, purple and green routes). These do not react chemically with hydroxyl groups of cellulose but block their ability to form hydrogen bonds with other hydroxyl groups. In derivatisation a reagent reacts chemically with hydroxyl groups and removes the possibility of hydrogen bonding. This intermediate may be either stabile and possible to isolate, or labile and needs to be processed immediately (Figure 1.3, left-side, yellow routes).

According to the definition of *coagulation*, a substance changes to a gel or thickened curdlike state from liquid through a change in environment (McGraw-Hill, 2003; Merriam-Webster, 2014). Cellulose derivatives can be *regenerated* back to cellulose by cleaving the functional group away and generating the hydroxyl groups (Figure 1.3, left route, pink box). After the cleavage, newly formed hydroxyl groups can form hydrogen bond networks, causing molecules to aggregate (pre-nucleation sites (Nichols et al., 2002)) and hence to coagulate. Some materials, such as cellulose acetate, can be dissolved in organic solvents (Klemm et al., 1998) and coagulate before regeneration by exchanging the solvent for water.

In the case of the direct solvents coagulation occurs directly when the solvent is either neutralised, diluted beyond the effective concentration or otherwise invalidated, for example by changing the temperature. The coagulation box in Figure 1.3 shows the hydrogen bonds of the 020 plane for the “up” chains, according to Kolpak and Blackwell (1976).

1.3.1 Derivatisation and dissolution

The most common cellulose derivative is cellulose xanthate (Klemm et al., 2005). It is prepared by activating cellulose with alkali and treating it with carbon disulphide CS_2. The xanthate group is thermally labile and cannot be isolated. After derivatisation cellulose xanthate is directly dissolved in alkali, when it becomes a viscose solution. After the shaping, the xanthate group

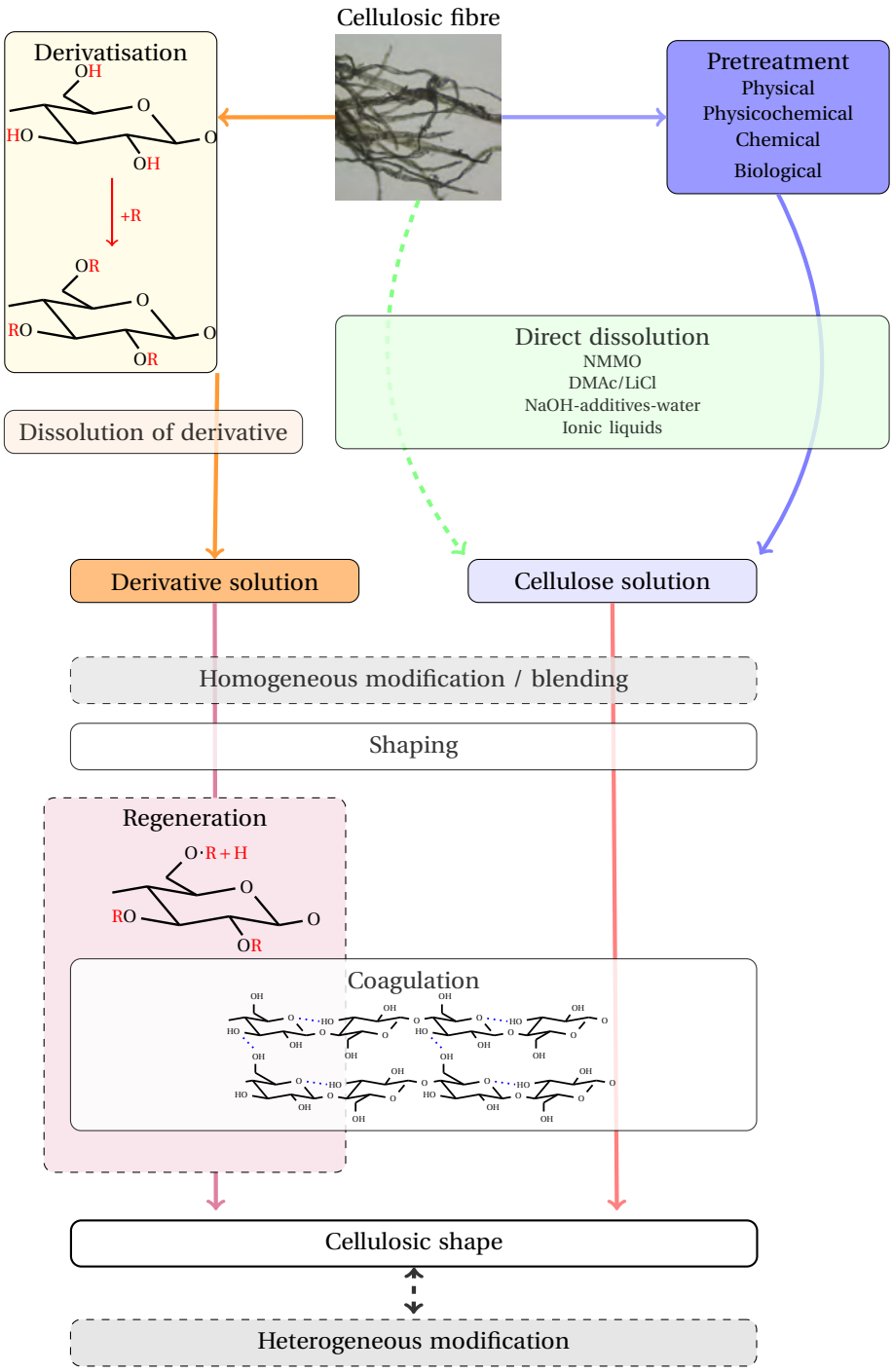

Figure 1.3: Schematic presentation of the processes from cellulosic fibres to novel shapes.

can be cleaved away with sulphuric acid or by thermal treatment, resulting regenerated cellulose.

Similarly, cellulose carbamate is formed when alkali-activated cellulose is in contact with molten urea (T>130 °C) (Loth et al., 2003). However, this intermediate is stabile and can be isolated. Cellulose carbamate is soluble in aqueous sodium hydroxide and can be regenerated with acid.

Another commonly used stabile derivative is cellulose acetate (Klemm et al., 1998). It can be isolated and is sold commercially with a wide range of degrees of substitution. It is soluble in organic solvents and thus polar solvents such as water can be used for coagulation. However, this does not cleave the acetyl group away and additional saponification is required if pure cellulose structure is desired. This opens the possibility of regeneration after the coagulation, as demonstrated by the long regeneration area in Figure 1.3.

1.3.2 Direct dissolution

Some conventional solvents dissolve cellulose directly without changing the chemistry of the hydroxyl groups. Most common non-derivatising solvent is used in the Lyocell process; *N*-methylmorpholine *N*-monohydrate (NMMO) (Fink et al., 2001). Since the solvent is very sensitive to moisture, water can be used to hinder its solvent abilities and to coagulate the cellulosic shapes. Another way to precipitate cellulose from an NMMO-solution is to let it cool to 20-40 °C from dispersion temperature >85 °C, so that crystallites are formed (Biganska et al., 2002). Unfortunately NMMO-solvent is also labile around impurities, so cellulose-blends with other polymers or additives cannot be prepared homogeneously (Konkin et al., 2008; Rosenau et al., 2001) and a solvent system requires stabilizers.

N,N-dimethylacetamide with lithium chloride (DMAc/LiCl) is more commonly used for homogeneous cellulose modifications (Heinze et al., 2006; Liebert, 2010). Water or acetone can be used as a non-solvent, although it is expensive and its recyclability is challenging. Other challenges with DMAc/LiCl include its high viscosity even with low amounts of cellulose (Kaster et al., 1993; McCormick et al., 1985). This makes it difficult to use in industrial processes, but it is well suited to academic research.

Ionic liquids (ILs) have gained a lot of interest since the beginning of new

Millenium (Gericke et al., 2012). They are defined as a group of organic salts which have a melting point below 100 °C. They can directly dissolve high amounts of cellulose, even 10-20%, but they can still, nevertheless, be used as a medium for dissolution and homogeneous derivatisation (Heinze et al., 2005; Kosan et al., 2008; Swatloski et al., 2002). Majority of ILs have dialkylimidazolium cations and various anions, e.g. 1-butyl-3-methylimidazolium chloride and acetate (BMIMCl and BMIMAc). Many of them, however, cannot dissolve cellulose (Gericke et al., 2012). Besides the advantages to efficiently dissolve cellulose, ILs have many unsolved issues; their properties can be drastically changed if there are even small amounts of impurities present, viscosity can increase even at low cellulose concentrations so that the solution is not suitable for processing, recyclability is still questionable, they can be difficult to purify, and some of them are chemically labile. However, research on novel ILs continues and many of these issues can be solved (e.g. King et al. (2011)).

Conventional water-based solvents are usually heavy metal salts and hydroxides. They form meta-stabile complexes with hydroxyl groups of cellulose and provide good solutions with relatively low viscosities. However, environmental restrictions strongly restrain their use on a commercial scale. Their use is still common for some standard measurements, such as the use of cupriethylene diamine for the measurement of the limiting viscosity number of pulp (standard ISO 5351).

Novel water-based solvents fulfill requirements in the areas of the environmental, health and safety (EHS) (Capello et al., 2007). In practice, these solvents are aqueous NaOH solutions with or without additives. Sodium hydroxide can dissolve cellulosic fibres with a low degree of polymerisation at low temperatures (Isogai and Atalla, 1998), although the solution is more a suspension than a true solution (Roy et al., 2003). To enhance solubility and delay the gelation time, additives such as urea (Cai and Zhang, 2005; Qi et al., 2008), thiourea (Jin et al., 2007), and zinc oxide (Liu et al., 2011), are added in solvent. Where sodium hydroxide swells and eventually dissolves cellulose, zinc and urea hydrates prevent the re-association of cellulose molecules and thus stabilise solutions.

1.4 Controlled release systems

New drug delivery systems have enabled new forms of therapies due to novel innovations, such as binding drugs to proteins for more targeted delivery and different release patterns (pulsating and continuous) (Langer, 1990). The advantages of a controlled delivery system becomes clear when the drug has a narrow therapeutic window, low dosage does not have the desired affect on a patient and high dosage is toxic.

Generally polymer-based matrices and coatings are used for controlled release effect (Vervaet et al., 1995). Depending on the physical or chemical properties of the polymer matrix, systems can be divided into three categories (Langer, 1993; Leong and Langer, 1988):

1. Diffusion controlled, non-degradating matrix.
2. Diffusion controlled, swelling matrix.
3. Erosion controlled, degradating matrix.

A drug can be coated with polymer, so that it diffuses through the polymer layer (Figure 1.4A). These are often called *reservoir systems* (Arifin et al., 2006). If the drug is evenly distributed, for example by dissolving and trapping the drug inside the matrix, or by dispersion, it is called a *matrix system* (Figure 1.4B). In the case of degradating matrices the drug is firmly bound to the matrix and is only released when the degradation occurs (Figure 1.4C). When simplified, degradation can happen via two routes; if the polymer chemically goes through a cleavage or scission, or in the case of erosion where it loses monomers or oligomers via a physical or chemical reaction. The erosion can occur only on the surface or through the entire bulk at the same time (Arifin et al., 2006). Cleavage of the drug from the polymer is one special type of this definition (Figure 1.4D).

Swelling systems (Figure 1.4E) usually utilise hydrophilic polymers, such as hydroxypropylmethyl cellulose (HPMC), poly(hydroxyethyl methacrylate) (HEMA) and poly(vinyl alcohol) (PVA), to enhance the swellability and solubility of poorly soluble substances (Arifin et al., 2006). At the outer-most region of the matrix, on the *diffusion layer*, the polymer also dissolves due to low concentration and weak entanglement, however, losses are small compared to surface erosion and do not play a role in the release rate of the drug.

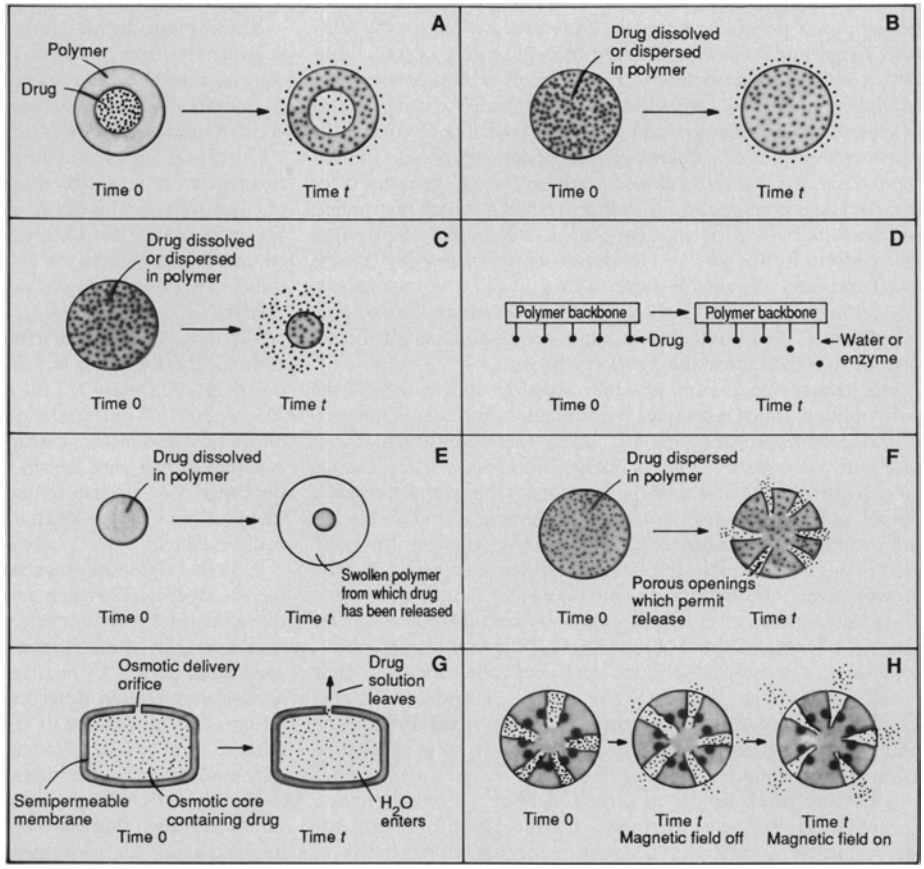

Figure 1.4: Different release mechanisms. (A) Diffusion through reservoir coated with polymer matrix, (B) drug uniformly distributed in matrix, (C) polymer degrades and releases the embedded drug, (D) contact with reagent or solvent in environment releases the linked drug from matrix, (E) polymer swells and allows drug to move outwards, (F) drug released only through porous holes, (G) drug is pushed out though the laser-drilled hole by osmotic pressure, and (H) release is activated e.g. by magnetic field squeezing the drug-containing pores. Figure from Langer (1990).

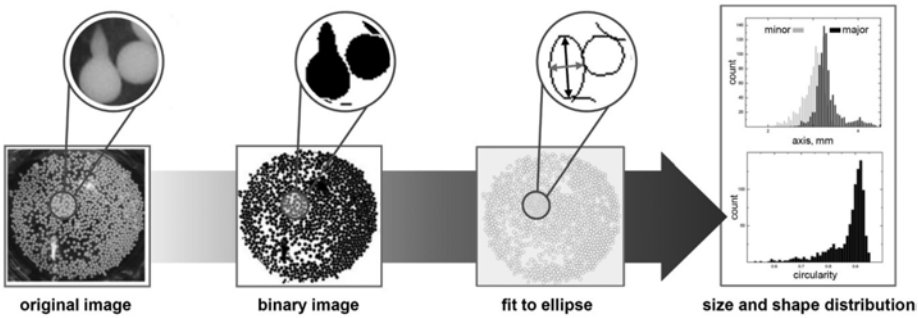

Figure 1.5: Image analysis of microspheres with Fiji software (Schindelin, 2008). Figure from Gericke et al. (2013).

Systems utilising osmotic pressure (Figure 1.4G) are a special type of diffusion controlled release system. Some systems are harder to categorise into one of the three types. Complex systems can often utilise properties from all three categories. In Figures 1.4F and H, osmotic pressure or external force may open the pores (partially degradating matrix), and diffusion occurs after they open in an otherwise stable matrix.

1.5 Characterisation of cellulosic shapes

Physical dimensions The physical dimensions and shape of the aerocelluloses and sponges are usually irrelevant in academic research, since their functionalities arise from internal properties. Spheres on the other hand use their size and shape as part of the functionality; loading capacity (see "Porosity and pore size distribution" section below), flowability, packing density, etc.

Spheres with a diameter of millimetres can be analysed simply by image analysis (Figure 1.5). Image analysis can be used, for swelling studies, for example, and as a complementary technique to determine total porosity (Trygg et al., 2013). A small bias may originate from the tail-formation and ellipse fitting of big spheres. Tails are formed when the highly viscose solution leaves the tip of the syringe and contacts the coagulation medium before minimising the surface energy, maintaining its tear-shape. Tails distort the fit to ellipse, prolonging the values of major axes. This is observed as a decrease in circularity values.

Smaller spheres of 10-1000 µm can primarily be analysed by sieving, although the results lack detailed information about the shape of the distribution (Rosenberg et al., 2007). Another option is to dry the beads, either under critical point drying, with liquid nitrogen or freeze-drying, and study the size and morphology with FESEM. Drying at ambient temperature, freezing and solvent exchange changes the size and possibly also the shape , however (Pinnow et al., 2008). This technique would give only indirect information about the original dimensions, but it also provides information about morphology and thus it is used rather regularly (e.g. Du et al. (2010); Trygg et al. (2013); Xia et al. (2008). Particle size analysers use laser light diffraction to measure the distributions of small particles in suspensions and provide a useful and rapid way to analyse the dimensions of micrometre sized particles (Thümmler et al., 2011).

Porosity and pore size distribution In the case of cellulosic shapes prepared by coagulation, it is likely that traditional models of pore shapes do not apply. Since the coagulation proceeds via gelation, the real pore structure is continuous matrix with channels of different widths. Thus the expression "pore size distribution" would be more precise if expressed as a total volume of channels of certain width in cellulose matrix. Some channels are narrower and thus some spaces are not accessible to all probe molecules, creating a combination of channels which can be called a pore.

The quality of the cellulose solution, the solvent and anti- or non-solvent all affect the coagulation mechanism and rate, which eventually determines the pore size distribution (Gavillon and Budtova, 2008; Trygg et al., 2013). Probably the biggest parameter affecting on the distribution and total porosity is the cellulose concentration in the solution; a defined space is filled with a certain amount of solids.

Total porosity can usually be measured at the same time as pore size distribution. In the simplest case one could compare the weights of wet and dried samples, and using a density of ~1.5 g cm^{-3} (Ettenauer et al., 2011) for cellulose it is possible to calculate the volume water occupied before drying (Xia et al., 2007). This does not, however, indicate the volume of *accessible* pores (Stone and Scallan, 1967, 1968).

Mercury intrusion or nitrogen adsorption techniques can be used as comple-

mentary tools for pore size distribution measurements; mercury intrusion measures pores from 3 nm to 200 µm and nitrogen adsorption from 0.3 to 300 nm (Westermarck, 2000). A disadvantage is that both measurements require a completely dried sample, which means critical point drying. Pressure is also applied to fill the pores against the surface tension of the filling material which can compress the closed pores and destroy the matrix during the measurement, yielding a higher volume of small and medium pores.

Pore size distribution can be measured in wet state, for example with small angle X-ray scattering (SAXS), which measures different electron densities between the pore wall and the water phase (Pinnow et al., 2008; Thünemann et al., 2011). This will also measure the closed pores. The solute exclusion technique with dextrans or polyethylene glycol (PEG) macromolecules measures only accessible pores for macromolecules of certain sizes (Figure 1.6)(Grznárová et al., 2005; Stone and Scallan, 1967, 1968). The concentration of macromolecules is measured before and after introducing the sample to the solution. If the water in pore is accessible to the macromolecule, it dilutes the solution. From the differences it is possible to compute the inaccessible and accessible volume fractions and relate them to the total volume. The total accessible pore volume can be estimated by extrapolating the size of the macromolecule to infinity. For dextrans the range is 1-56 nm and for PEGs 0.7-5.7 nm.

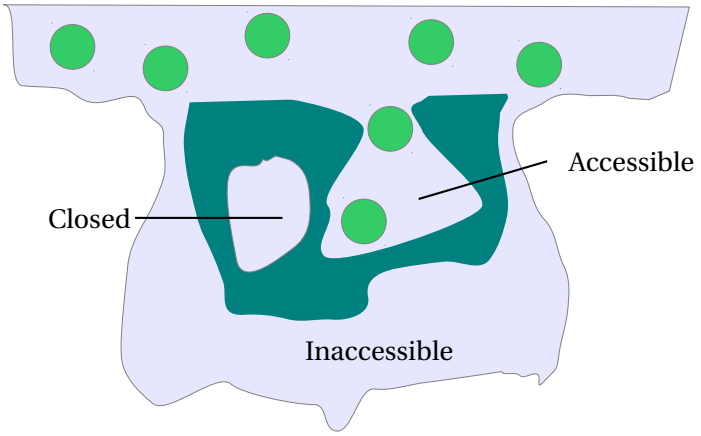

Figure 1.6: Illustration of accessible, closed and inaccessible pores by probe molecules. Adapted from Stone and Scallan (1968).

Specific Surface Area Specific Surface Area (SSA) becomes increasingly important if the cellulose shape is chemically modified heterogeneously after the solidification or sample is used in any application which is based on surface interactions, such as support in solid state synthesis, immobilisation or chromatographic separations with functional groups (Gericke et al., 2013). Whereas the surface area of the native cellulosic fibre varies between 55 and 168 m^2g^{-1} (Budd and Herrington, 1989) for dried and never-dried pulps, coagulated shapes can often have area over 200 and even as high as 450 m^2g^{-1} (Trygg et al., 2013). In regenerated fibre it is necessary to arrange the molecules in tight order for required elongation and strength, but in gelation the molecules fill up the given space. This maximises the porosity and area. However, after drying the surface area of the coagulated shapes can diminish to below 1 m^2g^{-1} due to a greater tendency to hornify (Trygg et al., 2013).

The techniques mentioned in the previous paragraph can often be used to measure the specific surface area as well. However, if the surface area is computed from the pore size distributions, rough assumptions and simplifications have to be made for the geometry of the pores (Stone and Scallan, 1968), which is contradictory to pore formation in gel-based shapes. If any dry technique, such as nitrogen adsorption or mercury intrusion is used, critical point drying may change the surface area (Svensson et al., 2013). This makes the techniques less comparable but they are often the only realistic option available.

Water retention value Water uptake and the ability to hold it are probably the most important properties of absorbent materials. Often standards SCAN-C 62:00 or DIN 53814 are used to measure the water retention value of chemical pulp fibres and textiles, respectively. They compare the mass of the wet sample to the mass of the oven dry sample. In SCAN-C 62:00 for example, the wet sample is centrifuged at 3000 G for 15 minutes to remove the surplus water. This method is mainly for pulp fibres, so for other sample types the method can be modified. Larger shapes such as sponges and spheres may be influenced by their own weight, and larger pore entrance allows water to leak out during centrifuging and thus the results might be distorted (Trygg et al., 2014).

Strength The strength of the cellulose matrix arises from the thickness of the pore walls. The thickness is again a result of coagulation kinetics and the amount of material available, that is the relationship between the anti- or non-solvent and solvent, and concentration of cellulose. Shape becomes stronger if a greater amount of cellulose occupies the volume, and simultaneously it decreases the volume of the pores and their size (Sescousse et al., 2011a). The formation of a thick supportive matrix can be jeopardized by blending other polymers in a cellulose solution which does not contribute to the matrix as intensively as cellulose, or by chemically modifying the hydroxyl groups.

Mechanical strength is usually measured by deformation under force and in practise this means stress-strain curves while compressing the sample. Together with the other results this provides information about the shape and its formation (Sescousse et al., 2011a). The bulk density can also be deducted from the mechanical characteristics (Pekala et al., 1990). In the case of wet samples, small spheres, and weaker shapes, applying centrifugal force and measuring the deformation by image analysis has also been proposed (Gericke et al., 2013), but this method has not been published in the literature yet.

Composition and functional groups Cellulose itself can be used as a functional material; it is biocompatible, it has three hydroxyl groups per repeating unit, and it forms an adjustable open-pore matrix and surface area. Other properties, such as flowability and total pore volume, can also be utilised. Many application, however, require ionic or hydrophobic interactions, for example. If the sample is functionalised for these purposes by blending with other polymers, composition becomes relevant and should be correlated to the other analysis methods mentioned above. The strength of the cellulose/polymer mixtures should also be ensured since the gel-matrix may not be supportive enough to maintain the shape (Wu et al., 2010; Zheng et al., 2002). For example, different polymer compositions can be analysed after acid hydrolysis or methanolysis using high performance layer chromatography or mass spectrometer-gas chromatography.

In the case of functional groups, such as anionic groups, titration methods are often applied. Either in conductive or potentiometric mode, titration provides direct information about the quantity of accessible groups and in latter mode possibly also the pK_a values of the acidic and basic groups. Other

methods for anionic groups are, for example, methylene blue and polyelectrolyte adsorptions (Fardim and Holmbom, 2003; Fardim et al., 2002). In the case of coagulated cellulosic shapes such as spheres and sponges, diffusion time would be too long to apply any direct or rapid method. Indirect titration and long equilibrium times must be used (Ettenauer et al., 2011; Trygg et al., 2014).

The distribution of such groups can be further located by labelling them with fluorescent dyes and using a confocal fluorescent microscope (Trygg et al., 2014), or by labelling anionic groups with methylene blue and locating the dye with ToF-SIMS. With methylene blue sorption it is also possible to measure the quantitative amounts of functional groups using isotherms.

Morphology Morphological study by FESEM is probably the most common technique in scientific publications. It provides *visual* information about the sample, its porosity, and morphological features (Du et al., 2010). Differences in coagulation mechanism, kinetics, and surfaces can also be observed in micrographs. The interface of gas and liquid, and later gelated solid surface was observed when a gas-forming agent was used inside the coagulating cellulose droplet (Figure 1.7). The distribution of different particles, such as inorganic metals, which cannot be fully blended in cellulose matrix can also be seen in cross-sections (Xia et al., 2007).

1.5.1 Characterisations for pharmaceutical applications

Powder flow Cellulose spheres utilise their shape as a part of their functionality. In pharmaceutical sciences the most common methods for measuring the properties of powders and spheres are angle of repose, compressability, flow rate through an orifice and shear cell (Chapter “1174. Powder Flow” in USP 29–NF 24, page 3017). All these methods measure the flow properties of a sample with or without external force. Additionally they provide information about shear-stress and friction, but these methods are all very much dependent on the apparatus used.

Angle of repose relates to the interparticulate friction between particles and resistance to movement, but it is not considered an intrinsic property of the solid. Powder is piled into a cone shape and the width of the base and the

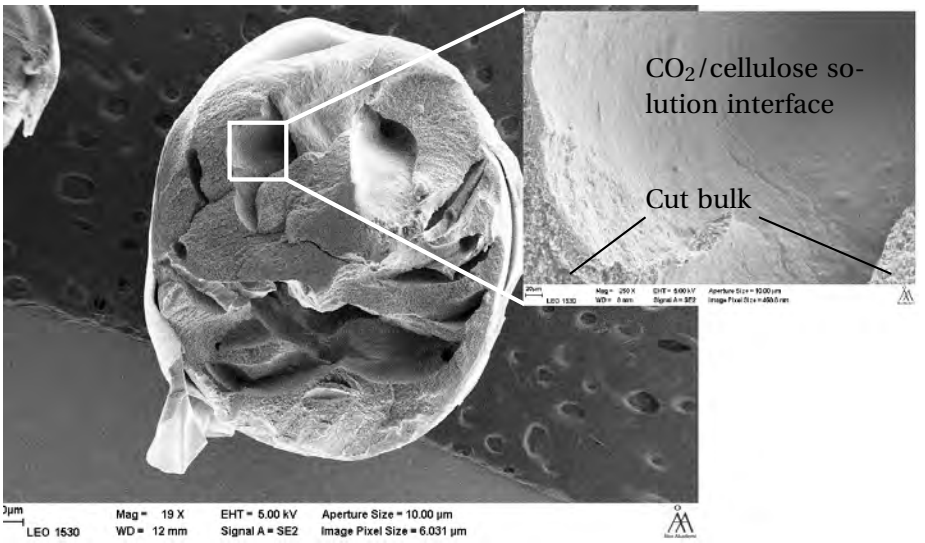

Figure 1.7: Interfaces of CO_2 and cellulose solution during the coagulation of cellulose microsphere. Sphere cut with blade, water exchanged to acetone and liquid CO_2 and then critical point dried prior to FESEM imaging. Magnifications 19× and 250×. Unpublished results.

height are measured from the pile. The angle is calculated from equation

$$tan(\alpha) = \frac{height}{0.5 \times base}. \tag{1.1}$$

The classification by Carr defines angles between 25-30° as excellent, and angles above 50° as poor, and rarely acceptable in pharmaceutical processes (Carr, 1965).

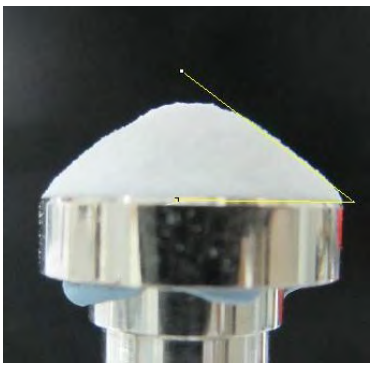

Figure 1.8: Angle of repose of dry cellulose beads.

The compressibility index and Hausner ratio are indirect measurements of bulk density, but they are also often related to moisture, size and shape, the surface area, and cohesiveness of the materials. They are both measured from the relationships of bulk volume to the tapped

volume. As angles of repose, they are not intrinsic properties of the material and are very dependent on the method used.

Flow through an orifice is used in free-flowing materials to measure the mass that flows in a defined time through an orifice. Flow rate is also often used. Since pulsating patterns and a decrease of the flow rate have been observed when containers empty, continuous monitoring is necessary.

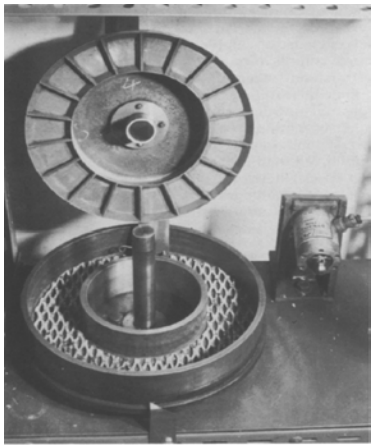

Figure 1.9: Old annular shear cell apparatus. Figure from Carr and Walker (1968).

Shear cell methods can measure several different parameters, such as shear stress-strain relationship, the angle of internal friction, yield and tensile strengths, and various flow factors. Powder is placed inside the apparatus, where one plane (or disc) is moving and other one is stationary. This generates a measurable stress on the sample.

Cell viability assay becomes increasingly important if the cellulose matrix is modified; Pure cellulose is biocompatible but derivatives might not be (Miyamoto et al., 1989). Aerocellulose and sponges are often used as wound dressing materials and scaffolds for new healing tissue (Lagus et al., 2013). Novel shapes must pass the test, since skin has to be able to heal but not to grow into the cellulose matrix, unless the matrix is simultaneously degrading.

2 Experimental

Dissolving pulp (Cellulose 2100 plus) from Domsjö Fabriken (Sweden) was used in this work. The pulp is a mixture of spruce and pine (60%/40%) and contains 93% α-cellulose and 0.6% lignin (Domsjö, 2007). The intrinsic vistosity of the pulp was 530±30 $cm^3\ g^{-1}$, measured according to SCAN-CM15:99. In Papers II-IV and Supportive Article 3 the pulp was pretreated with HyCellSolv-pretreatment for 2 h at 75 °C. The method is described in Paper I.

Paper II describes the preparation and modification of the cellulose microspheres (beads) using the physicochemical method. Paper III mainly focuses on the oxidation of the prepared spheres and the changes in their properties due to oxidation. Paper IV studies in detail the behaviour of anionic microspheres and their use in drug delivery.

2.1 Paper I: HyCellSolv-pretreatment and the solubility of the pulp

2.1.1 HyCellSolv-pretreatment

100 cm^3 of technical ethanol (92.5w%) and 4 cm^3 of 37w% hydrochloric acid (Merck KGaA) was preheated to 25-75 °C and 4.0 g of dissolving pulp was immersed in it for 0.25-5 h. After the treatment the mixture was poured into 900 cm^3 of cold distilled water, filtered and washed until pH was neutral, and left in 1 dm^3 of distilled water overnight to ensure the ethanol-acid had exchanged to water. The next day the pH was confirmed to be neutral and the pulp was filtered and dried in an oven at 60 °C overnight.

2.1.2 Changes in fibre surface morphology

The morphological changes in the surface of the fibres and the opening of the fibre cell walls in the reference and pretreated pulps (2 h at 25 and 75 °C) were examined using Leo Gemini 1530 FE-SEM with an In-Lens detector after coating with carbon in a Temcarb TB500 sputter coater (Emscope Laboratory,

Ashford, UK). An optimum accelerating voltage was 2.70 kV and magnifications were 5,000 and 50,000×.

2.1.3 Degree of polymerisation

Intrinsic viscosities were measured according to ISO/FDIS 5351:2009 standard and average degrees of polymerisation were calculated from the values (Immergut et al., 1953). Oven-dry samples were freeze-dried and weighed before dissolution in 1.0 M cupriethylene diamine solution (CED). The temperature of the capillary was 26.0 ± 0.1 °C.

2.1.4 Dissolution mechanism

Optical microscopy (Wild M20 coupled to a Nikon Coolpix 990 digital camera) was used to study the dissolution mechanism of the reference and pretreated pulps at various temperatures and times. 0.2 M CED was used to simulate weak solvent and slow dissolution. 0.2w% cellulose solutions were made using 7% NaOH-12% urea-water as a solvent and pretreated pulps after 2 h at 25, 45, 55 and 65 °C. The types of undissolved fragments were recognised from the solutions.

2.1.5 Solubility of cellulose in 7% NaOH-12% urea-water

The nature of the cellulose-7% NaOH-12% urea-water solutions was evaluated rheometrically. 0-5% cellulose (pretreated 2 h at 75 °C) was slurred in 7% NaOH-12% urea-water so that the fibers were swollen. The mixture was cooled to -10 °C and stirred until a clear solution was obtained, usually less than 20 minutes. An Anton Paar Physica MCR 300 rotational rheometer with DG 26.7 double-gap cylinder was used to measure the dynamic viscosities at 10, 15, 20, and 25 °C and the apparent activation energies E_a of viscous flow were calculated using Arrhenius equation (Roy et al., 2003). Shear rates of 10, 100 and 1,000 s^{-1} were used to study the state of the solution under different shear conditions.

Paper II: 4-6% cellulose was dissolved in 7% NaOH-12% urea-water as described above. Storage and loss moduli (G' and G") were measured at 20 and 25 °C with the same rheometer to define the gelation point of the solutions.

2.2 Paper II: Physicochemical design of the microspheres

2.2.1 Preparation of the physicochemically designed microspheres

Cellulose was dissolved as described in Section 2.1.5 with final concentrations of 3-7%. The solution was extruded through the Eppendorf 5 cm^3 syringe tip into the coagulation bath. The conditions were adjusted according to Table 2.1.

Table 2.1: Cellulose microspheres prepared under different conditions.

$c_{cellulose}$ (%)	T (°C)	c_{HNO_3} (M)	$c_{cellulose}$ (%)	T (°C)	c_{HNO_3} (M)	$c_{cellulose}$ (%)	T (°C)	c_{HNO_3} (M)
4	25	2	5	25	0.5	5	5	2
5	25	2	5	25	2	5	25	2
6	25	2	5	25	4	5	50	2
			5	25	6	5	5	*
			5	25	8	5	25	*
			5	25	10	5	50	*

* 10% NaCl was used instead of HNO_3

2.2.2 Dimensional attributes and morphological features

Physical dimensions, size distributions, and the shape of the never-dried microspheres were studied by analysing photographic images with Fiji image processing software (Schindelin, 2008). 20-100 microspheres were used in each analysis. Weight was measured before and after drying in an oven at 105 °C to determine the total porosity using equation

$$Porosity = \frac{V_{H_2O}}{V_{H_2O} + V_{cellulose}} \tag{2.1}$$

where V_{H_2O} is calculated from the mass differences of the wet and dry beads, and $V_{cellulose}$ from the dry mass of the beads divided by the density 1.5 g cm^{-3}.

The effect of the coagulation conditions (Table 2.1) on morphology was studied using a Leo Gemini 1530 FE-SEM with In-Lens detector. Never-dried microspheres were cut prior to acetone exchange and CO_2 critical point drying. Dried spheres were carbon coated before imaging with a Temcarb TB500

sputter coater (Emscope Laboratories, Ashfold, UK).

2.2.3 Intrinsic properties: pore size distribution and specific surface area

Pore size distribution of microspheres coagulated in 0.5, 2, and 6 M nitric acid at 25 °C and 10% NaCl solution at 5, 25, and 50 °C were measured using modified solute exclusion technique (Stone and Scallan, 1967, 1968). Approximately 4.0 g of never-dried microspheres in water (total weight 5.0 g) were introduced to precisely 5 g of 6% dextran solutions of five different molar masses, ranging from 6k to 2M g mol^{-1} (Table 2.2). After few hours of gentle shaking, the concentrations were measured using a Perkin-Elmer 241 Polarimeter with Na-lamp radiation source (589 nm). The inaccessible volume for each dextran was calculated using the equation

$$Inaccessible\ water = m_{water+beads} - m_{dry\ beads} + m_{solute} - \frac{m_{solute} \times c_{solute,0}}{c_{solute,f}} \tag{2.2}$$

where $m_{water+beads}$ is the total weight, $m_{drybeads}$ is the weight after drying at 105 °C overnight, m_{solute} the weight of the 6% dextran solution, $c_{solute,0}$ and $c_{solute,f}$ are the initial and final concentrations of the dextran solutions. Results were fitted to the logistic model using Origin Software (2002) and the saturation point was computed. Finally, the results were transformed to frequencies using equation

$$Frequency = \frac{Total\ accesible\ water - inaccessible\ water}{Total\ accessible\ water}. \tag{2.3}$$

Table 2.2: Molar masses and diameters of dextrans in solution.

Molecule	Molar mass (g mol^{-1})	Size (Å)
Dextrans	6k	39
	40k	91
	100k	139
	500k	290
	2000k	560

Nitrogen adsorption isotherms were measured at 77 K after CO_2 critical point drying (Section 2.2.2) using TriStar 3000 gas sorption apparatus (Micromeritics, Norcross, USA). Specific surface areas were determined from the adsorption isotherms using the equation by Brunauer et al. (1938).

2.3 Paper III: Chemical functionalisation of the microspheres

Cellulose microspheres were prepared as described in Section 2.2.1 using 2 M nitric acid at 25 °C and 5% cellulose solution. The needle used in this work was 50 mm long with a 0.8 mm diameter.

2.3.1 Anelli's oxidation

Microspheres were oxidised using a modified Annelli's oxidation (Anelli et al., 1987; Zhao et al., 1999). They were immersed in 50 mM NaH_2PO_4 phosphate buffer overnight prior to oxidation. TEMPO/NaClO/$NaClO_2$ oxidation medium was prepared with molar ratios 0.1/10/1, according to Hirota et al. (2009) in the same phosphate buffer. The medium was preheated to 20-80 °C and microspheres were immersed in for 2, 5, 24, and 48 h. pH was followed regularly. The ratio of the primary oxidant sodium chlorite $NaClO_2$ to anhydroglucose unit (AGU) of cellulose was 1.2. After oxidation, the microspheres were washed thoroughly under running tap water overnight and several times with distilled water. Oxidised microspheres were stored in distilled water in a never-dried state for further use.

Spectroscopic characterisation of the air-dried (2 days at 22.5 °C, 50% humidity) reference and oxidised microspheres was performed with a Nicolet iS 50 FTIR spectrometer with Raman module (Thermo Scientific). FTIR spectra were recorded using Tungsten-Halogen source and DLaTGS-KBr detector-splitter set-up with 4.00 cm^{-1} resolution and 64 scans. In Raman measurements a gold plate was used as a sample holder in order to strenghten the signal. A diode laser (P=0.5 W, λ=1064 nm) was the source and detector was an InGaAs with CaF_2 splitter. Resolution was 8.00 cm^{-1} and the number of scans 1024.

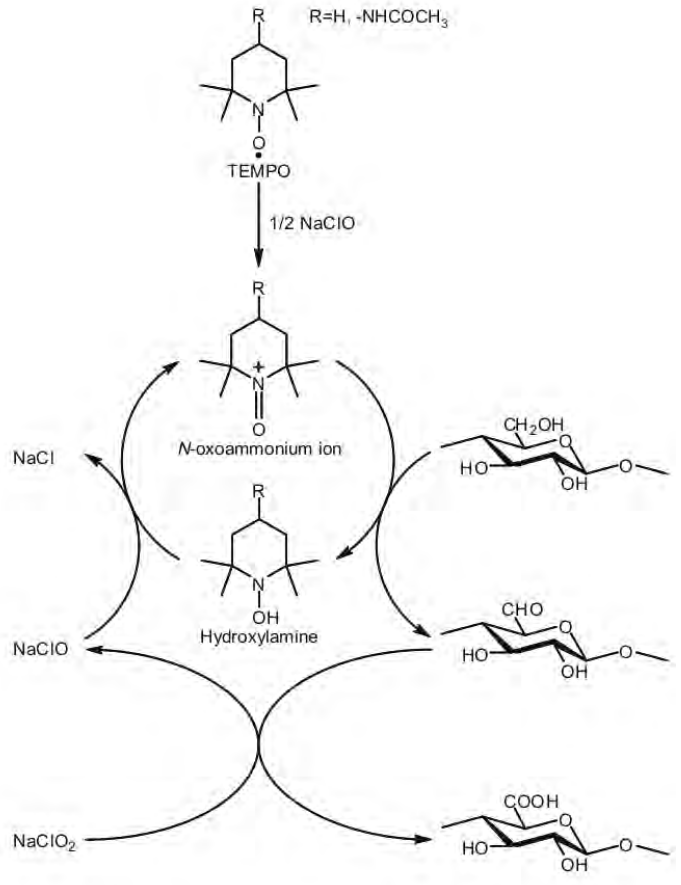

Figure 2.1: Oxidation-reduction cycle of reagents in cellulose-TEMPO/NaClO/$NaClO_2$ system. Figure from Hirota et al. (2009).

2.3.2 Porosity and pore size distribution

A solute exclusion technique was used (Section 2.2.3) to measure the changes in pore size distribution and accessible pore volumes when oxidation temperature was altered in 48 h oxidations. Total porosity was calculated using Equation 2.1 by weighing the samples before and after oven drying at 105 °C for three hours, as described in Section 2.2.2.

2.3.3 Distribution and quantity of the anionic groups

The distribution of the anionic groups was verified with cationic fluorescent dye, DMS. Oxidised microspheres were cut half, immersed in 15 µM DMS-solution overnight and next day washed for 4 h with tap water and distilled water to ensure the removal of unbound dye from the pores (Conn, 1953; Lonkar and Kale, 2011). The distribution was studied using a Leica TCS SP5 Confocal Microscope (Germany).

The quantitative number of anionic groups in oxidised microspheres was determined with potentiometric back titration. Due to the long diffusion time (≥30 min) direct titration was not possible. Microspheres were protonated by immersing them in hydrochloric acid solution overnight. The next day the concentration of the acid was titrated. The solution was alkalised and microspheres deprotonated by adding a known amount of sodium hydroxide. The next day the excess of alkali was titrated, and consumption of alkali by the anionic groups in microspheres was computed from the differences with the equation

$$n(-COOH) = (n(NaOH) - n(OH^-)) - n(H^+) \tag{2.4}$$

where n(-COOH) is the total number of anionic groups (mainly carboxylic acids), n(NaOH) is the added sodium hydroxide to neutralise the supernatant and to deprotonate the carboxylic acids, n(OH^-) is the back titrated amount of hydroxide after the NaOH addition, and n(H^+) is the back titrated amount of acid in the initial solution after the protonation (Figure 2.2).

2.4 Paper IV: Drug delivery with functionalised microspheres

The oxidised cellulose microspheres prepared in Paper III were used in this work. In Paper IV oxidised cellulose microspheres (beads) were labelled as OCBs, the number indicating the oxidation temperature and 0 the non-oxidised reference microspheres. Oxidation temperatures were 20, 40, and 60 °C and time was 48 h.

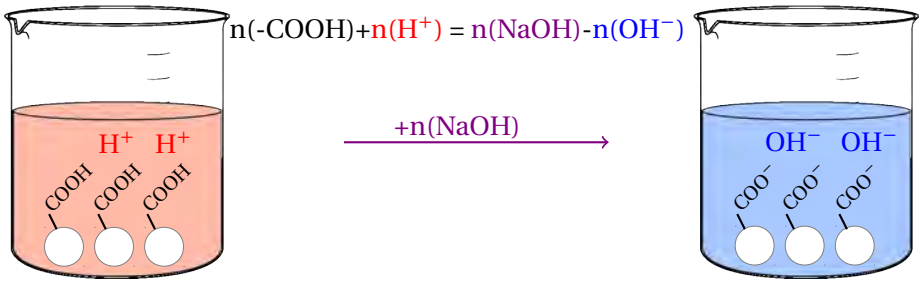

Figure 2.2: Determination of anionic groups (-COOH) from solids using the back titration method. The excess of acid (H^+) was measured by titration, then microspheres were deprotonated by adding NaOH and finally the excess of alkali (OH^-) was back titrated.

2.4.1 Drug loading and uniformity of the mass

ACBs were immersed in 20 mg cm^{-3} aqueous solution of Ranitidine hydrochloride (Ran.HCl) so that 2 microspheres were in 1 cm^3 of the drug solution. Vessels were gently shaken overnight. On the next day the loaded microspheres were surface dried by rolling them on glass plate until surplus solution was removed from the surface and then they were kept at constant temperature and humidity (22.5 °C, 50%) for at least 48 h.

Uniformity of the mass was studied by weighing the dried empty and loaded microspheres. The number of microspheres was increased by 5 between the weighings until the total count was 50. Linear correlation between the weight and the quantity was computed and the average weights were calculated from the slopes. The amount of the drug in the loaded microspheres was estimated from the differences in slopes.

2.4.2 Solid state analysis: ATR/FTIR and DSC

Dry ranitidine HCl loaded ACBs were analysed with ATR/FTIR and Raman spectroscopy (Nicolet iS 50 FTIR spectrometer with Raman module, Thermo Scientific; for details see Section 2.3.1) in order to characterise the polymorphic form of the incorporated drug and interactions between the anionic surface of the oxidised microspheres and cationic drug. In raman measurements samples were placed on a gold plate to obtain better signal/noise ratio.

Thermal analysis of 8-9 mg of empty and ~11 mg Ranitidine HCl loaded ACBs

was performed with DSC Q2000 (TA Instruments). Samples were placed in Tzero low-mass pans with lids and heated from 20 to 300 °C with 10 °C min^{-1} under 50 cm^3 min^{-1} flowing nitrogen.

2.4.3 Swelling behaviour of the microspheres

Empty and Ranitidine HCl loaded ACBs were dried at constant temperature and humidity (22.5 °C, 50%) for at least 48 h. Samples were then immersed in buffer solutions with pH values of 1.2, 3.6, and 7.4, corresponding to various environments in the human gastro-intestinal track. Swelling of the microspheres was monitored by imaging every hour for the first 5 hours, and finally after 24 hours. Images were analysed with Fiji imaging software (Schindelin, 2008) by fitting binary images to ellipses and measuring the length of the minor axes.

2.4.4 Release profiles

Release profiles were determined at pH 1.2, 3.6, and 7.4 in Sotax AT7 smart dissolution tester (SOTAX, Switzerland) according to the USP paddle method (United States Pharmacopeia, 35^{th} Ed.). Five drug loaded beads were sunk in 500 cm^3 of buffer solution at 37 °C and concentrations were measured using a Perkin-Elmer Lambda 25 UV/Vis spectrometer (Germany) and computed from calibration curves. Experiments were done in triplicate.

Release profiles were fitted to the model of exponential decay from 5 to 120 minutes with Qtiplot (2011). Y-offsets and e-folding times, that is the maximum released amount after infinite time and the time when approximately 63% of the total amount of the drug is released, were measured and compared with different bead types in various pH environments.

The effect of swelling on the release kinetics was studied by fitting the curves in two models: Baker-Lonsdale's model (Equation 2.5) for non-swelling monolithic spheres (Baker and Lonsdale, 1974) and Ritger-Peppa's model for swelling spheres (Equation 2.6, n=0.43) (Ritger and Peppas, 1987), where M_t and M_∞ are released amounts of drug at time t and infinite time, and k is the release

constant.

$$\frac{3}{2}\left(1-\left[1-\frac{M_t}{M_\infty}\right]^{\frac{2}{3}}\right)-\frac{M_t}{M_\infty}=kt \tag{2.5}$$

$$\frac{M_t}{M_\infty}=kt^{0.43} \tag{2.6}$$

3 Results and discussion

3.1 Paper I: Pretreatment and dissolution of cellulosic fibres

In HyCellSolv-pretreatment dissolving pulp was immersed in preheated 25-75 °C ethanol-acid -solution for 0.25-5 h. After the treatment pulp was thoroughly washed and dried in an oven at 60 °C overnight. The aim was to enhance the solubility of the cellulose in 7% NaOH-12% urea-water solvent system and characterise the significant changes in the properties of the pulp.

3.1.1 Morphological changes and degree of polymerisation: Influence on dissolution mechanism

Microfibrils in primary cell wall (P) do not have any specific orientation. This lack of orientation in microfibrils was observed in FE-SEM images of untreated dissolving pulp (Figure 3.1 A, B). Pulp treated with HyCellSolv for 2 h at 25 °C also showed disoriented microfibrils, but the surface was clearly damaged and the thin P-layer was not so clearly visible anymore (Figure 3.1, C, D). The secondary cell wall S1 is thinner than P, however, and could not be located with confidence (Jensen, 1977). After 2 h of HyCellSolv-treatment at 75 °C some remnants of the P-layer could be observed, but the orientation of the microfibrils mainly indicated that the outermost layer was secondary cell wall S2 (Figure 3.1, E, F).

Changes in the fibre wall after the HyCellSolv-pretreatment affected the dissolution mechanism of the pulp fibres in dilute solvent (Figure 3.2, optical images). At low temperatures (25-45 °C) and short treatment times a *ballooning* phenomenon was observed. This is explained in the literature as the presence of primary wall P and some parts of the secondary walls (Jensen, 1977; Navard et al., 2008). At higher treatment temperatures and longer times, for example 3 h at 55 °C ballooning was no longer so distinct, even though regions for possible balloons could be observed. After 5 h at 55 °C ballooning could no longer be observed. This was due to a ruptured P-layer and possibly

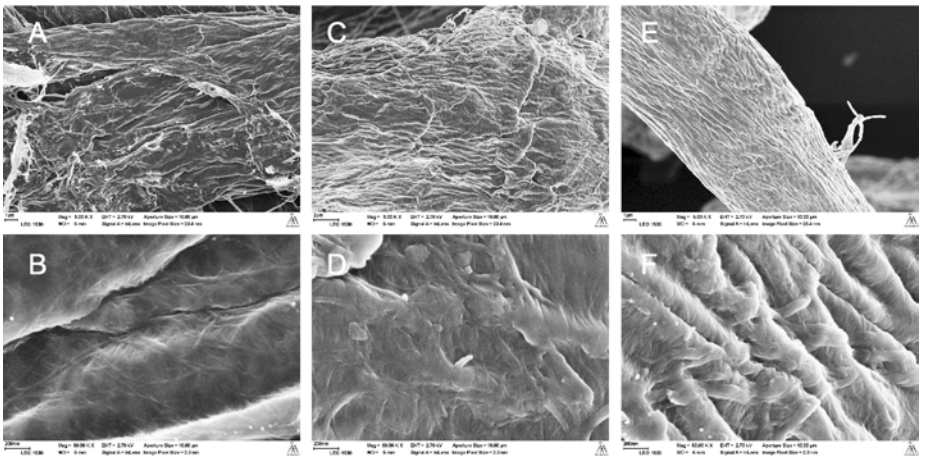

Figure 3.1: SEM-images of reference (A,B) and pulp treated with HyCellSolv for 2 h at 25 (C,D) and 75 °C (E,F). Magnifications are 5,000 in the top row and 50,000× in the bottom.

part of the S1 as well.

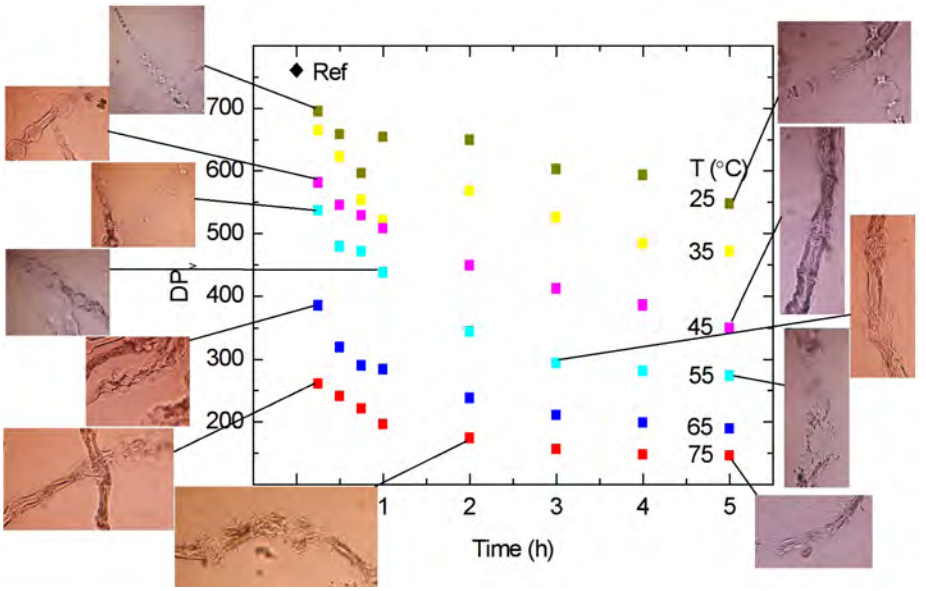

Figure 3.2: Viscosity average degree of polymerisation (DP_v) of HyCellSolv-pretreated dissolving pulp at various temperatures and times. Optical images demonstrate the behaviour of the fibres in 0.2 M CED after corresponding pretreatment conditions.

It should be noted that temperature alone did not eliminate the ballooning. HyCellSolv-pretreatment even at 75 °C for 15 minutes caused slight ballooning, although *fragmenting* was also observed (Figure 3.2). Since the presence of P-layer after 15 minutes at 75 °C in HyCellSolv was more clear than, for example, after 5 h at 55 °C, it is reasonable to conclude that rupture of the P-layer is not directly connected to the degree of polymerisation. According to the factory specifications (Domsjö, 2007) pulp has a lignin content of 0.6%. It could be speculated that the high lignin content of the thin P-layer requires more time to dissolve in HyCellSolv-solution than cellulose degrades in whole fibre. The content of hemicelluloses did not change notably during the pretreatment (Paper I).

After 15 minutes at 75 °C the average viscosity degree of polymerisation DP_v had decreased to 261, which was 34% of the initial (760). Slight ballooning, the presense of the P-layer, was observed at this stage. After 2 h of pretreatment at that temperature DP_v was 174 (23% from the initial) and dissolution proceeded clearly via fragmenting mechanism.

HyCellSolv-pulp was dissolved in NaOH-urea-water solvent (consistency 0.2%) after various pretreatment times. In microscope balloons or indicators of the ballooning phase during the dissolution were observed when pretreatment temperature was below 65 °C (Figure 3.3, A-C), however, clear solutions were gained when the pretreatment temperature was higher than 65 °C (Figure 3.3, D).

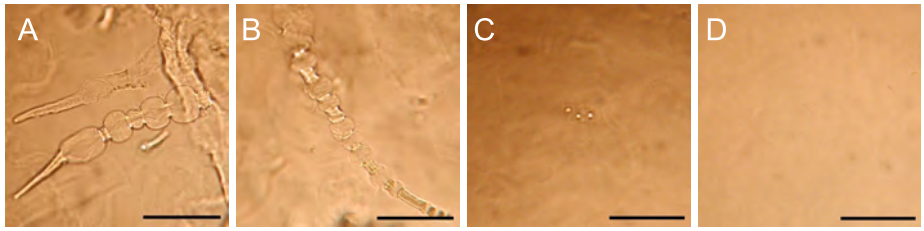

Figure 3.3: 0.2% HyCellSolv-pretreated pulp in 7% NaOH-12% urea-water. Pretreatment time 2 h and temperatures (A) 25, (B) 45, (C) 55, and (D) 65 °C. Scale bars are 100 µm.

It can be concluded that HyCellSolv-pretreatment at higher temperatures disrupted the primary cell wall and severely decreased the degree of polymerisation of cellulose. The lack of P-layer caused the fibres to dissolve via fragmenting mechanism instead of ballooning, yielding clear solutions with-

out "collars" (Figure 3.3, C) or other undissolved fragments. DP_v on the other hand did not play a significant role in the dissolution mechanism (e.g. in Figure 3.2 15 minutes at 75 °C or 3 h at 55 °C).

3.1.2 Nature of the 0-5% cellulose-7% NaOH-12% urea-water solutions

HyCellSolv-pulp (2 h at 75 °C) was dissolved in 7% NaOH-12% urea-water solvent system at -10 °C after dispersion and swelling at room temperature. Concentrations of cellulose were 0.2-5%, in order to study the nature of the solution.

At low concentrations the cellulose solutions behaved like Newtonian solutions, but at higher concentrations shear thinning was observed (Figure 3.4, left). The viscosity increased with increasing cellulose concentration and temperature. Since the viscosity of the solution is temperature dependent, it was possible to use the Arrhenius equation to calculate the apparent activation energies E_a for the viscous flow at extrapolated zero-shear rate and shear rates 10, 100, 1000 s^{-1}. Viscosities were plotted to Arrhenius plots and E_a values were computed from the slopes (Figure 3.4, right).

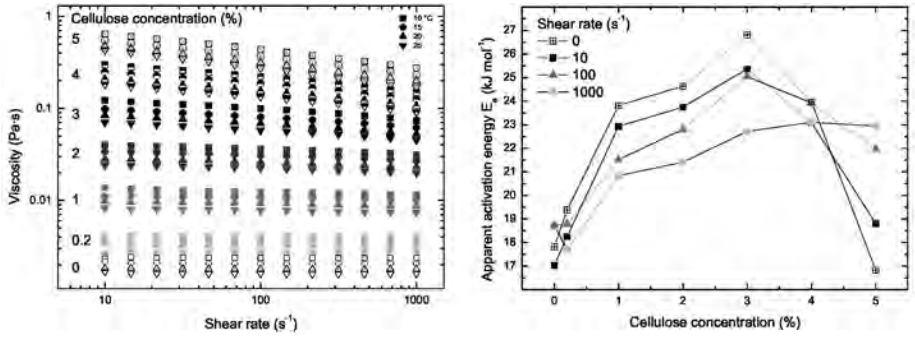

Figure 3.4: (Left) Viscosity of 0-5% HyCellSolv-cellulose in 7% NaOH-12% urea-water at 10-25 °C as a function of shear rate. (Right) Apparent activation energies E_a of viscous flow on shear rates 0, 10, 100 and 1000 s^{-1}.

At shear rates 0, 10, and 100 s^{-1} activation energies increase until the cellulose concentration exceeds 3%, then they decrease rapidly. This indicates the formation of the aggregates, or at least less resistant flow. Polymeric solutions should increase the resistivity to the flow with increasing polymer concentration. Addition of cellulose to the solution did not increase resistivity

to the flow, so the interactions between the polymer molecules were more prominent than with the solution. In this case, the addition of the cellulose decreased the activation energies rapidly, indicating strong aggregation and a decrease in interactions between the polymer and the solvent.

At high shear rate (1000 s^{-1}) activation energy increases slightly until 4% and remains constant at 5%. If the solution is a so-called "true solution", the activation energy should increase, however, activation energies did not decrease as at other shear rates. This is due to high shear, where the movement of the molecules inhibits the formation of the stable aggregates.

Cellulose is often dissolved in aqueous alkali solvents at reduced temperatures. One explanation for this is the formation of inclusion complexes, which inhibit the coagulation of the molecules (Lue et al., 2007; Qin et al., 2013). Collapse of the inclusion complexes occurs at elevated temperatures and gelation, the formation of the hydrogen bonding network begins. When the network is strong enough, the storage modulus takes over and the solution becomes more gel-like than a viscous solution.

4-6% cellulose solutions were heated to 20 and 25 °C and storage (G') and loss (G") moduli were measured as a function of time (Figure 3.5). At 25 °C 4% cellulose solution gelated after 28 minutes and the 5% solution 5 minutes earlier. The 6% cellulose solution had already gelated after 8 minutes when temperature was 25 °C. When the 6% solution was studied at 20 °C, gelation took 33 minutes, clearly longer than even a 4% cellulose solution. This supports the results of Qin et al. (2013) that at higher temperatures inclusion complexes are fully destroyed and cellulose molecules are exposed to the formation of hydrogen bonds with each other.

It should also be noted that at the concentrations used in gelation studies, only a 4% cellulose solution could have been near a "true solution" state. Others already contained some H-bonded cellulose molecules, however, the fact that 6% gelated 25 minutes later when the temperature was lowered below the degradation point of the inclusion complexes indicates that these aggregates were surrounded by NaOH-urea-hydrates and could not coagulate.

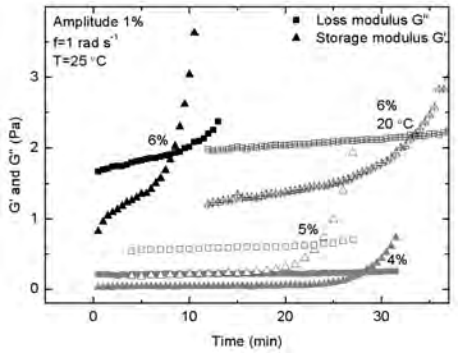

Figure 3.5: Storage and loss moduli of 4-6% cellulose-7% NaOH-12% urea-water solutions. Cross-sections of the moduli indicate the gelation points.

3.2 Paper II: Physicochemical design of microspheres

3-7% cellulose-7% NaOH-12% urea-water solution was prepared from HyCellSolv-pulp (pretreatment 2 h at 75 °C) and the solution was extruded drop-wise through a syringe (Eppendorf 5 cm^3) into the conditioned antisolvent (Table 2.1). The aim of the study was to demonstrate the effect of the coagulation conditions on the properties of the microspheres. A 3% cellulose solution could not form stable microspheres due to a lack of the building material. Moreover, the 7% solution was too viscous to form droplets and formed a continuous flow instead.

3.2.1 Size, shape, and weight of microspheres

The size of a microsphere is defined by the size of the droplet detaching from the needle through which it is extruded. Shape, on the other hand, can be influenced by several factors. Depending on the cellulose concentration in the dope, during the detachment from the needle the droplet stretches and forms a tail. Higher cellulose concentration causes more stretching (tailing).

Another factor affecting the shape is the impact with the antisolvent. If the needle is too far from the surface, the surface tension of the antisolvent causes an impact which flattens the droplet (Sescousse et al., 2011b). Conversely, if the needle is too close to the surface, the droplet may attach to it after passing through the surface. Since the droplet is still denser than the antisolvent, it tends to fall to the bottom. Attachment on the surface and gravity together

stretches the coagulating droplet and forms a tear-shaped microsphere.

The size of the cellulose microspheres increased when the 5% cellulose solution was coagulated in 2 M nitric acid and 10% NaCl solution at increasing temperature (Figure 3.6A, Table 3.1). The same trend was observed with increasing acid concentration (Figure 3.6B). Faster coagulation kinetics under these conditions caused the skin layer to solidify immediately after the contact with antisolvent and maintain the initial dimensions of the droplet. As the coagulation kinetics slowed down by decreasing temperature or acid concentration, the interior parts of the droplet had more time to pack more closely and the ongoing coagulation inside of the microsphere pulled the outer layers closer and caused slight shrinking.

Table 3.1: Gaussian parameters of normalised size distribution values from images of cellulose microspheres prepared under different conditions

Preparation conditions			Gaussian parameters	
$c_{cellulose}$ (%)	T (°C)	c_{HNO_3} (M)	Peak (mm)	FWHM [a]
4	25	2	2.92	0.16
5	25	2	2.97	0.16
6	25	2	2.99	0.20
5	25	0.5	2.71	0.32
5	25	2	2.97	0.16
5	25	4	2.67	0.60
5	25	6	3.02	0.58
5	25	8	3.05	0.27
5	25	10	3.31	0.41
5	5	2	2.41	0.37
5	25	2	2.70	0.24
5	50	2	2.85	0.21
5	5	[b]	2.79	0.32
5	25	[b]	2.76	0.24
5	50	[b]	3.20	0.14

[a] Full width at half maximum
[b] 10% NaCl was used instead of HNO_3

Circularity, i.e. $4\pi \times$area/perimeter^2, was found to be unaffected by the increased acid concentration, but the increased temperature yielded slightly

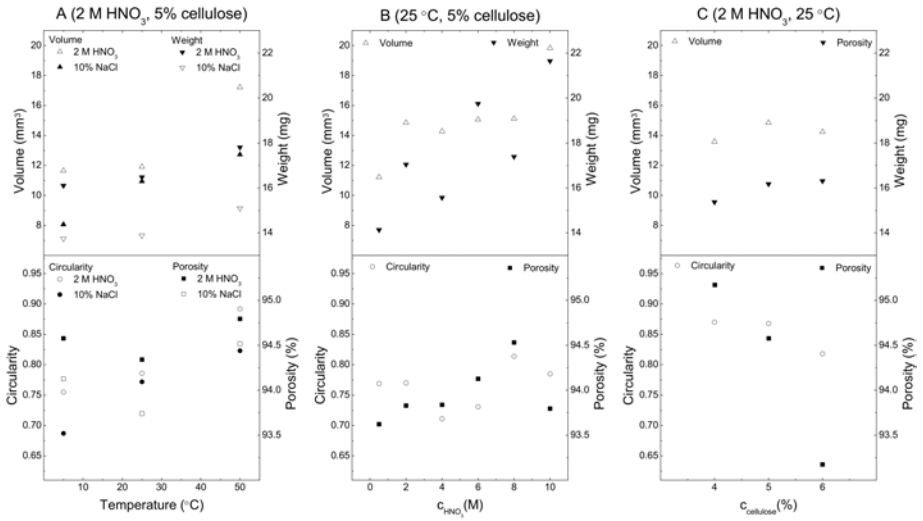

Figure 3.6: The effect of (A) temperature, (B) acid concentration and (C) cellulose concentration on volume (△ ▲), weight (▼ ▽), circularity (∘ •) and porosity (■ □). Constant parameters are given above the figures.

more spherical particles. The surface tension of the acid increases with the concentration (Weissenborn and Pugh, 1996). This accelerated the formation of the skin layer and droplets maintained their shape after the first contact with the acid. When the temperature of the antisolvent was increased from 5 to 50 °C, the surface tension decreased by 10% (Vargaftik et al., 1983). A lower surface tension assisted the droplet in passing through the surface boundary without attaching to it and tail-formation was minimised.

The weight of the microspheres closely followed the volume. Porosity again follows these two values closely, since it is calculated from the amount of water in certain volume. When the cellulose concentration was increased (Figure 3.6C), more solid material occupied the same volume. A slight increase was observed in volume and weight (density of the cellulose is ~1.5 g cm^{-3}). This caused the porosity to decrease rapidly.

3.2.2 Morphology of the cross-sections and surfaces of the microspheres

Slow coagulation in milder acid formed more coarse surfaces than fast coagulation in concentrated acid (Figure 3.7). Fast coagulation inhibited the

formation of bigger agglomerates, and fibrils can be seen on the surface of the microspheres coagulated in 2-10 M nitric acid solution. Faster coagulation also yielded smaller fibrils (Figure 3.7B-D).

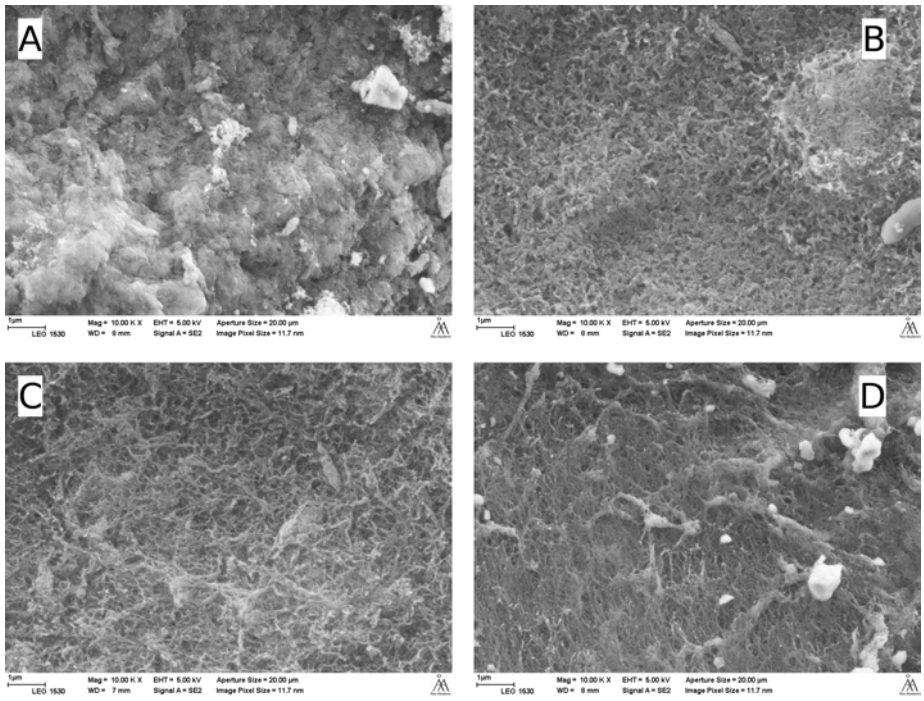

Figure 3.7: FE-SEM images of the surface of the microspheres. 5% cellulose solution coagulated in (A) 0.5, (B) 2, (C) 6 and (D) 10 M HNO_3 at 25 °C. Magnification is 10,000×.

Similar changes were observed in interior parts of the cross-sections (Figure 3.8). When coagulation was slower the size of the agglomerated fibrils was greater. Since the concentration changes of the antisolvent are not so severe inside the microspheres, the presence of the agglomerates was observed in microspheres coagulated in 2 M nitric acid. However, 6 M HNO_3 did not produce agglomerates any more and only fibril-like shapes were seen in cross-section images (Figure 3.8C).

The thickness of the skin layer was noted to increase when more concentrated acid was used for coagulation (Figure 3.9). In 0.5 M HNO_3 skin layer was hardly detectable, whereas in microspheres coagulated in 2-6 M HNO_3 it was ~3-6 µm thick. The coagulation mechanism was observed to change when 10 M acid was used; instead of simultaneous solidification (sol-gel transition)

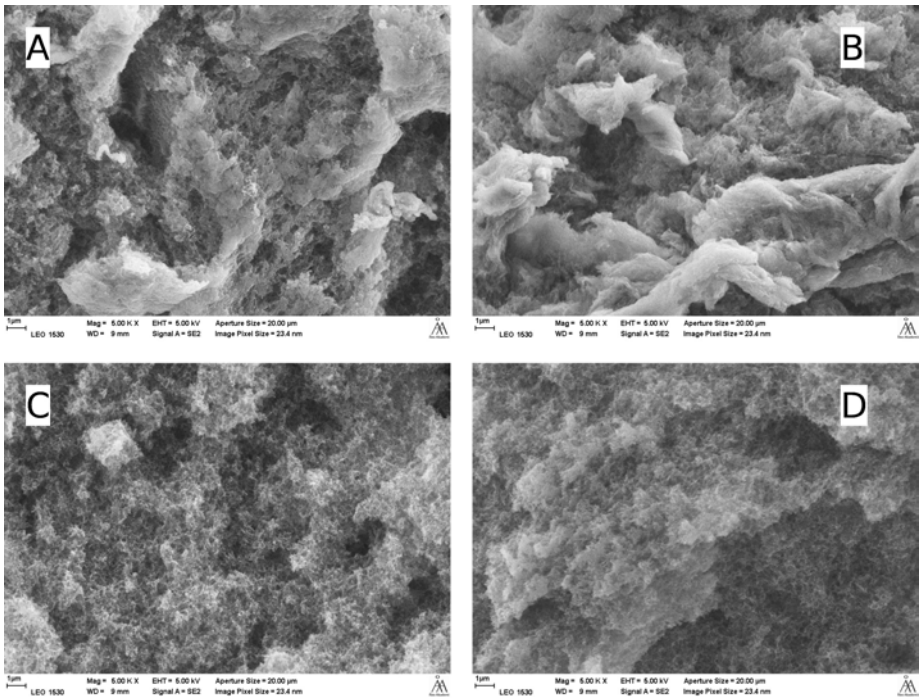

Figure 3.8: FE-SEM images of the interior of cross-sections of the microspheres. 5% cellulose solution coagulated in (A) 0.5, (B) 2, (C) 6 and (D) 10 M HNO_3 at 25 °C. Magnification is 10,000×.

from the surface towards the interior, several nucleation centres were formed on the surface of the droplet immediately after the contact with acid. Locally this formed "plates" which could even be ~50 µm thick, but the plates would not cover whole microsphere as continuous layer. The whole sphere was labile and they could not handle physical pressure or stress as well as spheres coagulated from milder acid environments.

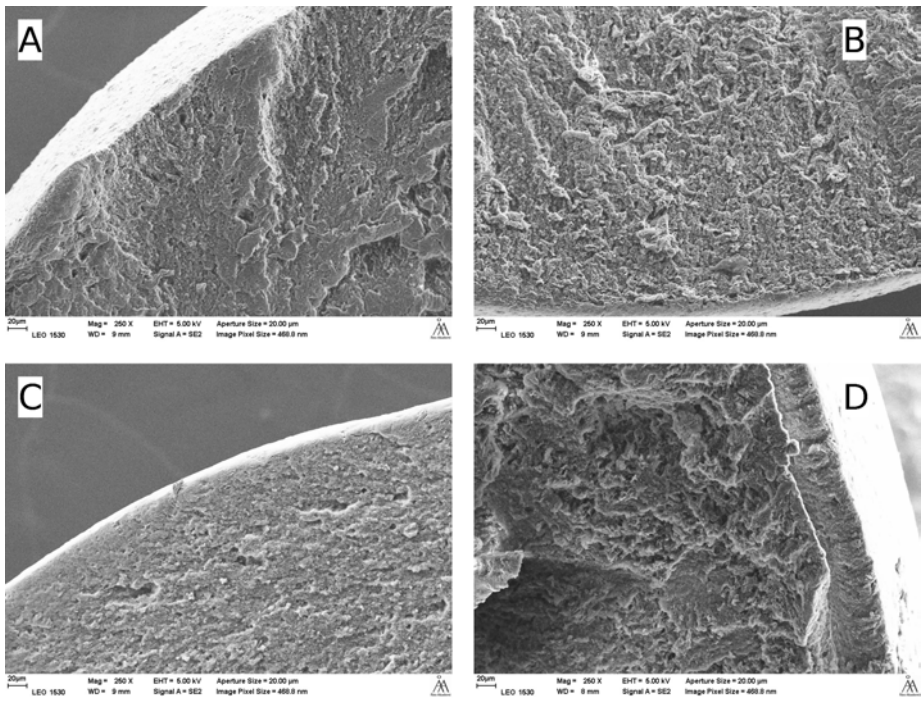

Figure 3.9: FE-SEM images of the edge of the cross-sections of the microspheres. 5% cellulose solution coagulated in (A) 0.5, (B) 2, (C) 6 and (D) 10 M HNO_3 at 25 °C. Magnification is 250×.

The surfaces of the microspheres prepared from 4 and 6% solutions and coagulated in 2 M HNO_3 at 25 °C were very similar to those prepared from 5% solution in same antisolvent (Figure 3.10). A skin-core structure was also observed in cross-sections on the edge. In microspheres prepared from 6% solution thicker structures were seen under the surface compared to microspheres prepared from 4% and 5% solutions. The pores were smaller in images showing the interior, and conversely in microspheres from the 4% solution pores were bigger. This observation is in agreement with the total porosity values (Figure 3.6, C) which decreased over a few per cent with increasing cellulose concentration in solution. This was explained by the

addition of solid material into a constant volume.

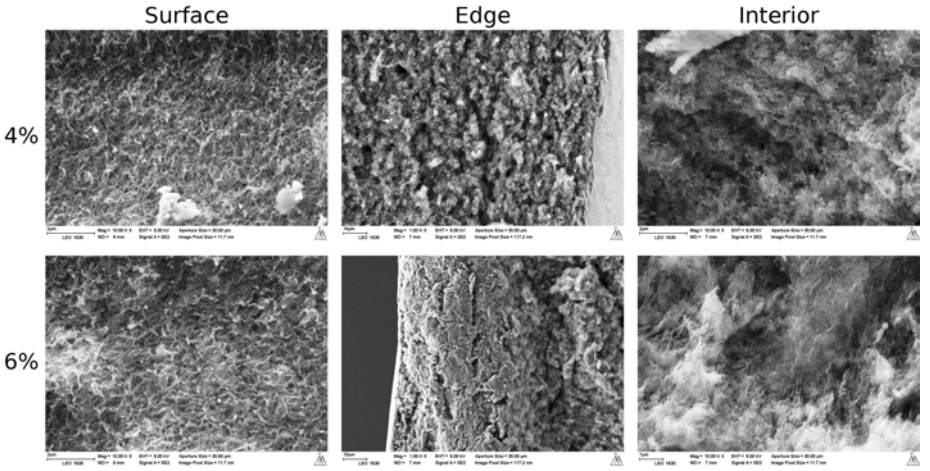

Figure 3.10: FE-SEM images of the surface, edge and interior of the CPD cellulose microspheres coagulated in 2 M HNO_3 at 25 °C. Magnifications are 1,000 (edge) and 10,000× (surface and interior).

3.2.3 Intrinsic properties

Pore size distribution

Pores of the cellulose microspheres were probed using dextrans of various molar masses (Table 2.2). The amount of inaccessible water was computed from the concentration differences (Equation 2.2; Figure 3.11, left) and converted to frequencies for each dextran (Equation 2.3; Figure 3.11, right).

The total accessible water (the saturation point) for all the samples varied between 91% and 92% (Figure 3.11, left). This is clearly lower than reported in Figure 3.6. The difference results from the closed pores and limited range of dextran probes; the smallest dextran used in this study can access the pore with an entrance of 36 Å, which then excludes all the micropores (<20 Å) and even some of the small mesopores (Westermarck, 2000).

When the acid concentration of the antisolvent was increased, coagulation kinetics increased and macropores (≥560 Å) were favoured over mesopores (39-290 Å; Figure 3.11, right:top). Slower coagulation gave cellulose molecules more time to arrange themselves to fill the whole space (sol-gel transition), which also maximised the specific surface area (Figure 3.12, B). The sum of

the mesopores (0.5 M 0.669; 2 M 0.649; 6 M 0.598) follows a nearly linear trend and is inversely proportional to the frequencies of the macropores (0.276, 0.289, 0.348).

When the microspheres were coagulated in 2 M acid but at different temperatures, kinetics did not explain the variations in pore size distributions (Figure 3.11, right:bottom). Similar trends as with macropores in this measurement were, however, observed in total porosity values (Figure 3.6, A:bottom, solid squares). Coagulation at 25 °C produced microspheres with the lowest porosity and amount of macropores. Since the volume (Figure 3.6, A, top, open triangles) was almost the same at 5 and 25 °C coagulated microspheres, the higher amount of mesopores and lower amount of macropores resulted from the faster movement of the cellulose molecules at higher temperature, and thus more even spreading across the constant volume. However, the sol-gel process did not take over due to the elevated temperature (note the gelation point, Figure 3.5) but was still a result of the neutralisation.

At 50 °C, however, coagulation was so rapid that the skin layer solidified faster than at lower temperatures and generated microspheres with higher volume (Figure 3.6, A, top, open triangles) and higher frequency of macropores (Figure 3.11, right: bottom). It should be noted that surface area decreased with increasing temperature (Figure 3.12, A), so generally the same explanation as for the increase of the acid concentration applies here; fast coagulation packed the cellulose molecules more tightly to clusters, creating bigger pores and less coverage over the space. It could be assumed that the sol-gel process played a bigger role at 50 °C than neutralisation of the solvent by antisolvent.

Specific surface area

As observed in the subsection “Pore size distribution”, the amount of small mesopores increased when coagulation kinetics was slower (Figure 3.11, right: top). The specific surface area (SSA) increased when microspheres were coagulated at lower temperatures or in lower concentrations of acid (Figure 3.12, A and B), however, coagulation in 10% NaCl solution did not produce slightly lower SSA compared to HNO_3 even though coagulation kinetics was notably slower. The trend was very similar in both, anti- and non-solvents.

The increase in SSA when 8 and 10 M HNO_3 was used could be explained by a competing coagulation mechanism, as pointed out in Section 3.2.2 (Mor-

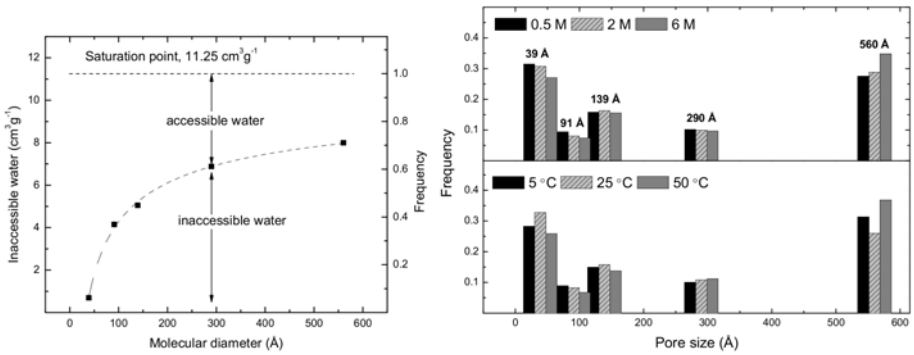

Figure 3.11: (Left) Inaccessible water, saturation point and frequencies of the pores of the microspheres coagulated from 5% cellulose solution in 2 M HNO_3 at 25 °C. (Right-top) Computed pore size distributions from the solute exclusion measurements for microspheres coagulated in 0.5-6 M HNO_3 at 25 °C and (right-bottom) 2 M HNO_3 at 5-50 °C.

phology of the cross-sections and surfaces of the microspheres). Decreased mechanical stability was observed while handling the microspheres. This also indicates that the supportive thicker pore walls did not have time to form and thus the microspheres became weaker than the ones prepared in lower acid concentrations. A high acid concentration probably resulted in smaller precipitates in the matrix and degraded some of the supportive structures.

When the cellulose concentration was decreased in the initial cellulose solution to 4%, a clear decline was observed in SSA compared to the microspheres prepared from 5% and 6% solutions (Figure (3.12, C). Assuming that the surface area in the microspheres produced from 5% solution was already just about maximised, less material in apparently the same volume (Figure 3.6, C: open triangles) undoubtedly yields less SSA. In the same manner it could be concluded that the addition of the material (6% solution) cannot increase already maximised SSA; further additions of cellulose would not only cause more aggregated molecules in solution (Section 3.1.2) but also less porosity (Figure 3.6, C). However, higher cellulose concentration yielded continuous stream of the solution through the needle and microspheres could not be produced. Conversely, less than 4% cellulose in the solution could not form solid and mechanically stabile spheres in antisolvent.

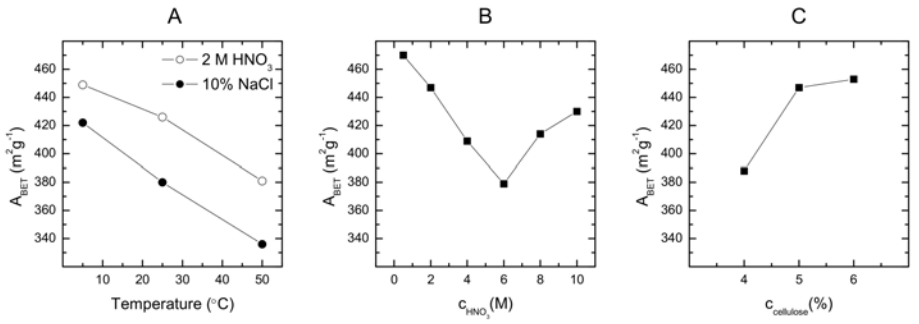

Figure 3.12: The effect of (A) temperature, (B) acid concentration, and (C) cellulose concentration on specific surface area of the critical point dried cellulose microspheres. General conditions for coagulation were: 5% cellulose solution coagulated in 2 M HNO_3 at 25 °C.

3.3 Paper III: Chemical modification of microspheres

Cellulose microspheres were prepared by dropping 5% cellulose-7% NaOH-12% urea-water solution into 2 M HNO_3 at 25 °C through the needle and oxidised with a modified Anelli's reaction. The aim of this work was to study the structural changes in microspheres after heterogeneous modification. Paper III also introduced the swelling properties of the oxidised microspheres and their application as drug carriers, but these are presented with more detail in Section 3.4 Paper IV: Drug delivery.

3.3.1 Oxidation mechanism and the amount of generated anionic groups

Microspheres were oxidised with a TEMPO/NaClO/$NaClO_2$ system (TEMPO-mediated oxidation) in phosphate buffer. Sodium chlorite $NaClO_2$ acted as a primary oxidant converting aldehydes into carboxylic acids at C6 position in cellulose (Hirota et al., 2009). There was an excess of $NaClO_2$ compared to AGU with a ratio of 1.2, which is in theory enough to convert all the C6 hydroxyl groups to carboxylic acid but in practise higher amounts of chlorite should be used to gain even water-soluble conversion yields (Hirota et al., 2009).

Oxidation in a TEMPO/NaClO/$NaClO_2$ system produces hydrogen ions (Isogai et al., 2011), however, an increase in pH values was observed during the

reaction when the reaction temperature was set to 60 and 80 °C (Figure 3.13). At 60 °C an increase occurred after 24 h but at 80 °C it occurred after 5 h. It is known that N-oxoammonium salt degrades under acidic conditions into TEMPOH, oxoammonium radical, and open ring carbocation at elevated temperatures (Ma et al., 2011; Sen and Golubev, 2009) (Figure 3.14B). Generation of additional TEMPOH to oxoammonium cation leads to increased consumption of hypochlorite and the production of hydroxide ions (Figure 3.14A). Primary alcohols are not oxidised to aldehydes since oxoammonium cations are degradating, hydrogen ions are not produced and the solution alkalises.

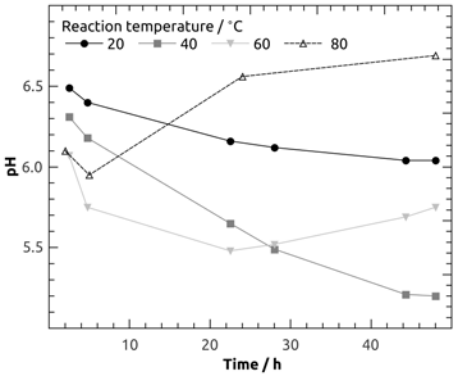

Figure 3.13: (A) Oxidation of primary alcohols to aldehyde by oxoammonium and TEMPOH intermediates in NaClO-water solution. (B) Degradation of oxoammonium salt at high temperature. Images adapted from Isogai et al. (2011) and Ma et al. (2011).

The total number of anionic groups which are protonated and deprotonated between pH values 2 and 11 were determined by back-titration method (Figure 3.15). At 60 °C oxoammonium ion degraded after 24 h, but it produced the highest amount of carboxylic acid groups in cellulose microspheres. At 80 °C yield was notably lower, probably due to a too high degradation rate at the beginning of the reaction and non-specific oxidation by hypohalous acid (de Nooy et al., 1995).

At 40 °C the decrease in pH value is the most notable (Figure 3.13). This indicates fast oxidation of cellulose and degradation of N-oxoammonium ions. Zhao et al. (1999) optimised the reaction temperature to 35 °C to reduce the chlorination in Anelli's reaction (Anelli et al., 1987).

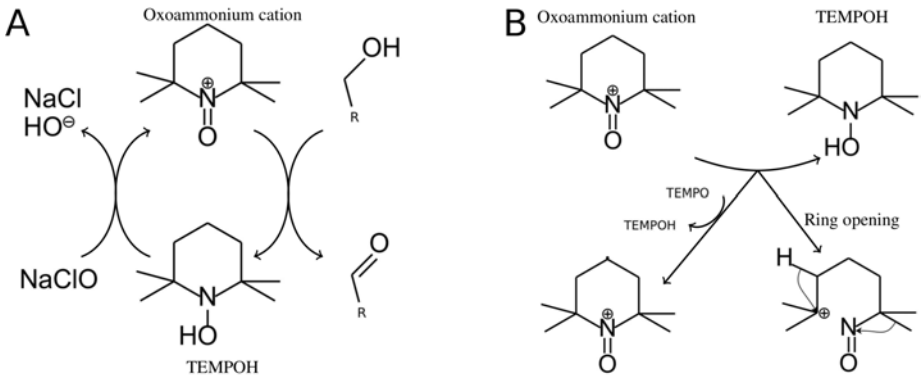

Figure 3.14: (A) Oxidation of primary alcohols to aldehyde by oxoammonium and TEMPOH intermediates in NaClO-water solution. (B) Degradation of oxoammonium salt at high temperature. Images adapted from Isogai et al. (2011) and Ma et al. (2011).

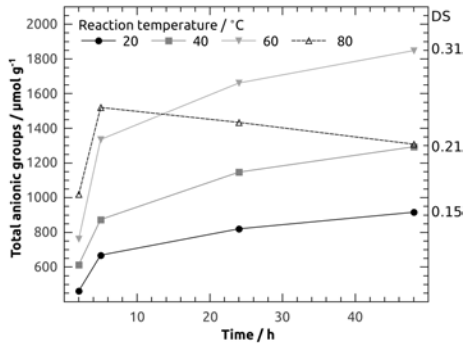

Figure 3.15: Total anionic groups in oxidised cellulose microspheres after 2-48 h of oxidation at 20-80 °C. Degree of substitution (DS) values correspond to the values after 48 h of oxidation.

3.3.2 Spectroscopic qualification and the distribution of anionic groups

Spectra of oxidised and reference microspheres were assigned according to the literature (Larkin, 2011) (Figure 3.16). Polymorphic type cellulose II was confirmed with Raman vibration at 1463 cm^{-1} (Schenzel and Fischer, 2001). Vibrations at the transition region around 1266 cm^{-1} were also perceived only for cellulose II but were not characterised exactly. Vibrations at 894 (FTIR) and 898 cm^{-1} (Raman) were assigned for δHCC and δHCO angle bendings around C(6) atom, semi-circle stretchings. This band is broader in cellulose I

and has multiple peaks due to different molecular conformation (Schenzel and Fischer, 2001).

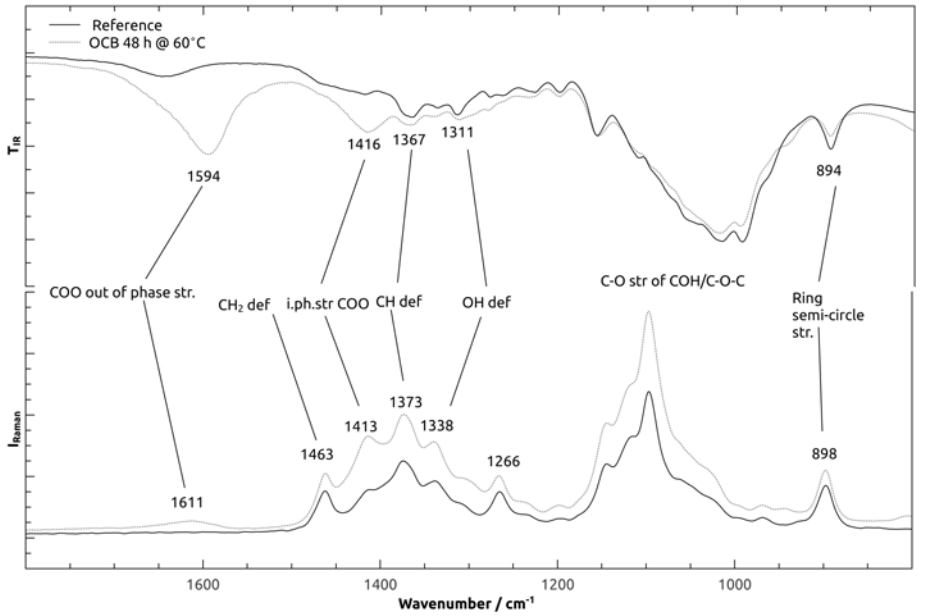

Figure 3.16: (Top) FTIR and (bottom) Raman spectra of reference and at 60 °C oxidised cellulose microsphere (OCB; oxidised cellulose bead).

The differences between reference and oxidised microspheres is the most profound at the region where R-COO vibrations are found; at 1400-1600 cm^{-1} in FTIR and 1400-1650 cm^{-1} in Raman spectra (Figure 3.17). The intensity of the R-COO vibrations increased almost linearly with oxidation temperature (Figure 3.17, insets), as long as the reference was excluded. Since intensities correlated well with the measured amount of total anionic groups (Figure 3.15) FTIR/Raman could be used for preliminary quantitative determination of AGs, as long as good internal standard is available. The phase stretching of R-COO in the FTIR spectra at 1416 cm^{-1} (Figure 3.17, left, open square) especially correlated with coefficient R^2=0.9995 without any lateral shift of the peak. Peak at 1594 cm^{-1} shifted when oxidation temperature was increased from 20 to 60 °C ($\Delta\nu$=5.3 cm^{-1}), probably due to underlying H_2O vibrations at 1640 cm^{-1}. The intensity of Raman peak at 1611 cm^{-1} was too low for precise quantitative analysis and 1413 cm^{-1} had a correlation of R^2=0.89 due to overlapping vibrations from CH_2 deformation (Figure 3.17, right).

Never-dried cross-sectioned microspheres were immersed in 15 µM DMS

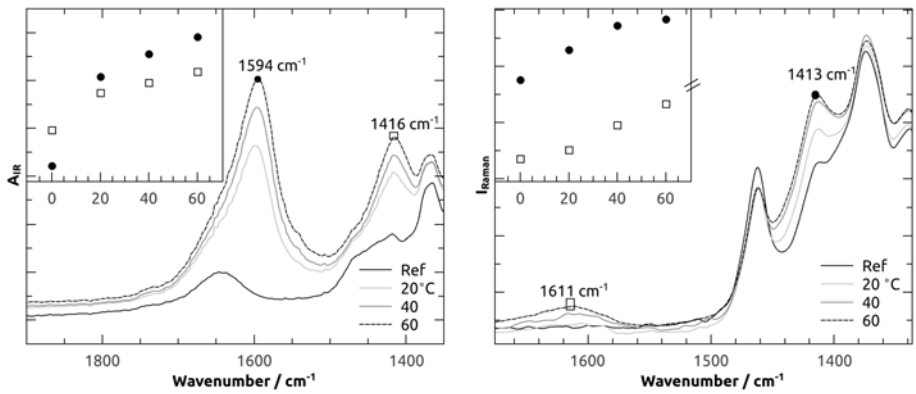

Figure 3.17: (Left) FTIR and (right) Raman spectra at specific regions for R-COO vibrations. Insets are showing the relative intensities of indicated peaks of microspheres oxidised at 0 (reference) and 20-60 °C.

solution overnight in order to label the anionic groups. Samples were washed thoroughly with tap water and distilled water to ensure that fluorescent dye would be bound only by strong ionic interactions and the excess would be washed away from the pores.

The distribution of fluorescent dye was observed with a confocal microscope (Figure 3.18). The slightly anionic surface of pure cellulose microspheres bound some of the dye, but a clear difference to the oxidised microsphere was confirmed with the same parameters of the excitation laser and detector. In both samples anionic groups, the bound DMS giving the response signal, were evenly distributed. A confocal microscope also revealed some of the morphological features in stack images (Figure 3.18, right).

3.3.3 Structural changes

Cellulose forms agglomerates during the coagulation. Bigger and more dense shapes are formed if the coagulation process is slow (Section 3.2.2 and Figure 3.19A,B). After oxidation in TEMPO/NaClO/$NaClO_2$ for 2 and 48 h at 80 and 60 °C, respectively, dense agglomerates were found to be more open and cloudy (Figure 3.19C-F). Intensive oxidation breaks the hydrogen bonding network by converting C(6) hydroxyl groups into carboxylic acids and at higher temperatures it may also degrade cellulose chains (de Nooy et al., 1995) and open the matrix, widening the pore entrances and cavities.

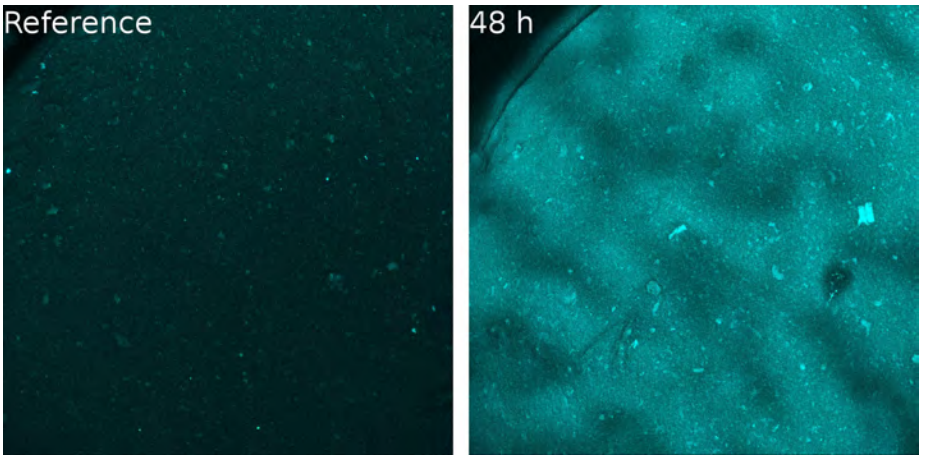

Figure 3.18: Confocal micrograms of cross-sections of (left) pure and (right) 48 h at 60 °C oxidised cellulose microsphere labelled with fluorescent cationic dye DMS. Images are 1.55×1.55 mm.

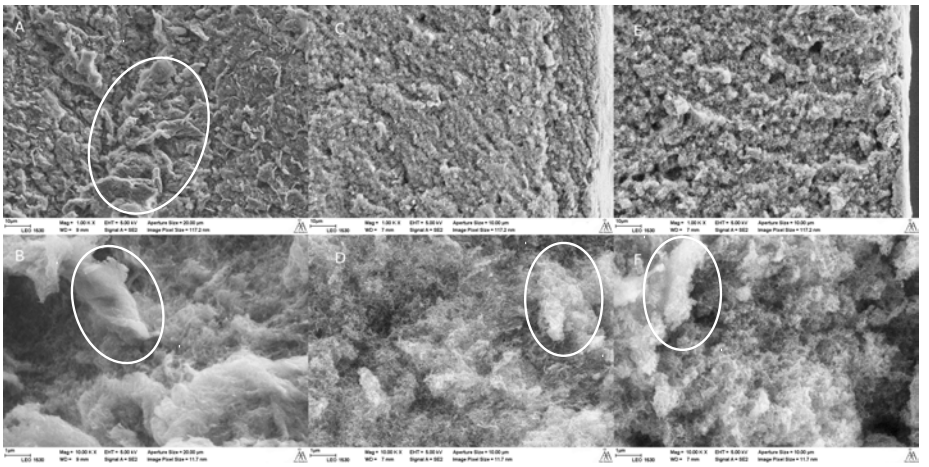

Figure 3.19: Micrograms of cross-sectioned CO_2 critical point dried (A, B) reference, (C, D) 2 h at 80 °C and (E, F) 48 h at 60 °C oxidised microspheres. White ovals highlight some of the agglomerates. Magnifications are 1,000 in the top row and 10,000× in the bottom.

Dextran molecules with various molar masses (Table 2.2) were used in a solute exclusion technique to probe the pores. Macropores (diameter ≥560 Å) had the highest frequency of all measured pores sizes (Figure 3.20). After oxidation for 48 h at 20-60 °C the relative amount of macropores decreased linearly (R^2=0.96) with increasing temperature. Contrary to the macropores, the sum

of the frequencies of small mesopores (39-139 Å) increased linearly (R^2=0.98).

Since the total porosities were all between 94-95% regardless of the oxidation temperature (Paper III, supplementary material) and the amount of accessible water for dextrans increased steadily from 82.28% to 84.37% in reference and oxidised microspheres at 20-60 °C, respectively, it is reasonable to hypothesise that small pores (small meso- and micropores) became wider and closed pores were opened during the oxidation. This enlarged the accessible volume for dextrans but did not change the total porosity.

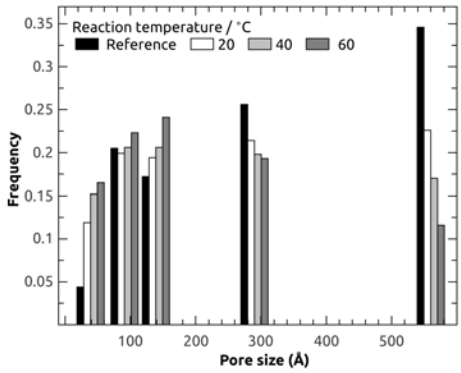

Figure 3.20: Pore size distribution of cellulose microspheres before and after oxidation in TEMPO/NaClO/$NaClO_2$ system for 48 h at 20-60 °C.

3.4 Paper IV: Drug delivery

Cellulose microspheres were prepared and oxidised as described in Papers II and III. The microspheres were assigned as ACB0-60, where 0 stands for reference cellulose beads and 20-60 anionic cellulose beads oxidised for 48 h at 20-60 °C. The aim of this work was to study the mass uniformity of the loaded drugs and the effect of the anionic charge on the loading and release profiles of cationic model drugs. To better understand the release mechanism, the behaviour of the dried microspheres was studied in physiological pH environments.

3.4.1 Uniformity of mass and drug content

The weight of microspheres is mainly defined by the volume of droplets and the cellulose content in solution. Since the cellulose content does not very

within the batch, the only variable is the volume. A droplet detaches from the tip of the needle when the viscosity of the solution cannot hold the growing weight of the droplet any longer. Since the viscosity does not notably change if the temperature of the solution does not drastically vary (Figures 3.4 and 3.5), the volume of the droplet is in a large extent constant.

The benefit of the immersion method over, for example, the dispersion method is that the loading degree can be adjusted by controlling the concentration of the solution and it will be the same for the whole batch. In the dispersion technique microspheres were loaded in 20 mg cm^{-3} Ranitidine HCl solution overnight and dried at constant temperature and humidity for two days. The mass of the batch of loaded and placebo ACBs was weighed by adding 5 microspheres until the total count was 50. Correlation coefficient R^2 for linear fit was over 0.999 in all measurements (Figure 3.21), indicating a very even volume and loading capacity.

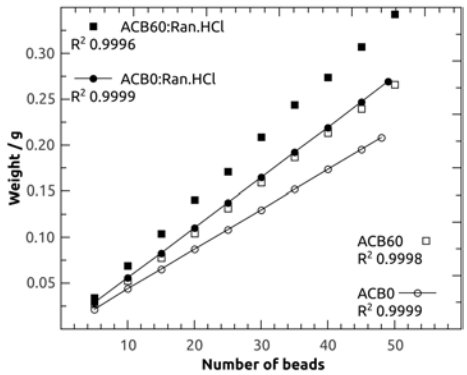

Figure 3.21: Uniformity of masses of loaded and placebo microspheres.

The amount of ranitidine hydrochloride was calculated from the differences in the slopes of the linear correlations (Table 3.2). The amount of drug increased in the microspheres when the oxidation temperature was increased. However, the high mass of placebo ACB60 was due to bound water (see Section 3.4.2) and thus the seemingly lower amount of drug than for example ACB40. Released amounts confirm that the actual drug content is higher than measured with gravimetric comparison (see Figure 3.26).

Even if the exact mass of loaded drug in microsphere cannot be determined by gravimetric methods alone due to odd amounts of bound water, high linear correlations demonstrate the uniformity of the microspheres and their

Table 3.2: Weights of placebo and loaded microspheres, amount of Ranitidine HCl per one microsphere and loading degrees. Calculated from the slopes of linear correlations.

	Weight / mg		Ran.HCl / mg	Loading / %
	Placebo	Loaded		
ACB0	4.33±0.01	5.46±0.01	1.13±0.01	20.7
ACB20	5.43±0.04	6.61±0.04	1.18±0.07	17.8
ACB40	5.09±0.02	6.86±0.06	1.77±0.08	25.8
ACB60	5.34±0.03	6.83±0.05	1.49±0.07	21.8

loading.

3.4.2 Solid state analysis

DSC measurements were performed after drying the ranitidine hydrochloride loaded and placebo microspheres at constant temperature and humidity for two days. Increased hydrophilicity of the placebo ACBs was observed as endothermic dehydration peaked at 200-225 °C (Figure 3.22). Dehydration began at lower temperatures as the peak area, the amount of bound water, increased in the microsphere. After the dehydration microspheres started to depolymerise 10-20 °C later (Dahiya and Rana, 2004).

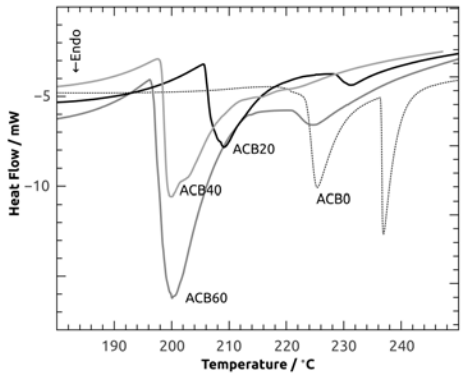

Figure 3.22: DSC of ACBs. Heating rate 10 °C min^{-1} and nitrogen flow 50 cm^3 min^{-1}.

Crystalline ranitidine hydrochloride has a melting point of 147 °C and it goes through exothermic decomposition instantly after the melting (Perpetuo et al.,

2013). The melting point was not observed when ranitidine hydrochloride was incorporated in the ACBs, indicating that it was solidified in amorphous form (Figure 3.23).

The changes in the intensities of the dehydration peaks are minimal compared to those of the placebo microspheres, indicating at least partial replacement of the bound water by the drug in loaded microspheres (Figure 3.23). Simultaneously with the incorporation of the drug, the stability of the microspheres decreased so that oxidised ACBs seemed to dehydrate already at 185 and ACB0 at 200 °C.

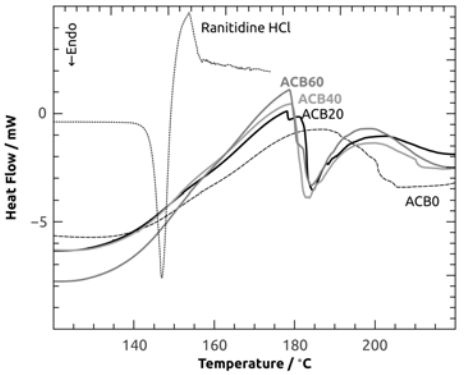

Figure 3.23: DSC of pure ranitidine hydrochloride and loaded ACBs. Heating rate 10 °C min^{-1} and nitrogen flow 50 cm^3 min^{-1}.

The crystal structure of the ranitidine hydrochloride was recognised as polymorph II by the characteristic region in the Raman spectra around 3000 cm^{-1} (Figure 3.24, inset) and the peak at 1185 cm^{-1} (Chieng et al., 2009). When ranitidine hydrochloride was incorporated in ACB60 and ACB0, the peak at 1555 cm^{-1} widened and shifted to 1552 cm^{-1} and the peak at 1185 cm^{-1} disappeared (Figure 3.24, ACB0 not shown). This is due to the amorphous form of the drug.

There were no changes in FT-IR spectra of oxidised ACBs when drug was incorporated (Figure not shown). The phase stretching of R-COO group at the region 1400-1650 cm^{-1} (Figure 3.17) in loaded ACBs did not change, indicating the lack of interaction between the cationic drug and the microspheres.

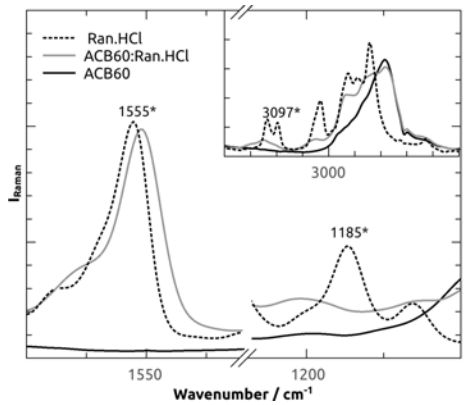

Figure 3.24: Raman spectra of Ranitidine HCl and ACB60 with and without incorporated drug. Inset: specific region 2750-3200 cm^{-1}. Symbols are characteristics for the polymorph II of Ranitidine HCl.

3.4.3 Swelling behaviour of placebo and loaded microspheres

Never-dried ACB0-20 had a diameter of 4.2 ± 0.2 and ACB40-60 4.3 ± 0.2 mm whether they were loaded with ranitidine hydrochloride or not. After drying the drug loaded microspheres were slightly bigger than the placebo ones; 1.8 ± 0.2 and 1.7 ± 0.2 mm, respectively (Trygg et al., 2014).

ACB0 swell very little in any tested pH environment (Table 3.3). After 24 h in buffer solutions ACB0 swelled to almost 50% from the initial never-dried diameter. Swelling at pH 1.2 was noted to be slightly higher than pH environments 3.6 and 7.4, regardless of whether the microsphere was loaded with drug or not.

Oxidised ACBs were approximately the same size after drying as ACB0, but the swelling behaviour at all tested environments was more intense. Even at pH 1.2, which is clearly below the pK_a of carboxylic groups, the microspheres swelled more than ACB0. Microspheres swelled up to 88% from the initial state when the oxidation temperature was increased to 40 °C. After oxidation at 60 °C the diameter of the drug loaded microsphere reached almost 90%.

Swelling mechanism was influenced by the drug loading in oxidised ABCs (Figure 3.25). For example, ACB60 without incorporated drug (Figure 3.25, open square) swelled during the first hour at pH 3.6 and 7.4 to the same point as ACB0 with drug, but instead of levelling-off ACB60 increased the swelling rate and the swelling continued for two hours before the rate decreased.

Table 3.3: Swelling of ACB0 and oxidised ACBs after 24 h at pH values 1.2, 3.6, and 7.4. Values are percentages from the diameter of corresponding never-dried CBs.

	Placebo				Loaded			
	Dry	1.2	3.6	7.4	Dry	1.2	3.6	7.4
ACB0	41.2	49.8	48.5	48.4	47.5	54.6	52.7	49.5
ACB20	41.4	52.7	59.5	72.8	47.3	57.3	63.2	78.0
ACB40	40.3	51.0	60.6	84.2	48.4	58.4	66.5	88.3
ACB60	41.5	50.0	64.8	88.0	47.7	55.9	64.2	89.7

After the wetting stage, *water infusion*, ACBs could increase their diameters throughout the sphere without causing any tension. ACB0 swelled during the first hour in all pH environments to its maximum value with and without the drug, as did the oxidised ACBs at pH 1.2.

A wetting stage was not observed when oxidised ACBs were loaded with drug and immersed in pH 3.6 and 7.4 environments (Figure 3.25, solid square). Slow down after one hour could not be observed, but instead swelling rate increasing immediately from immersion in the buffers until levelling-off 1.5-2 h from the beginning. The incorporated drug acted as a filler and pores stayed open. Wetting the pores occurred as fast as highly soluble drug dissolved away.

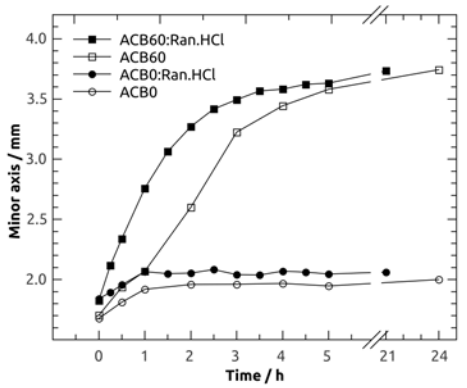

Figure 3.25: Swelling of the ACB0 and ACB60 with and without ranitidine hydrochloride at pH 7.4. The height of the ordinate indicates the average diameter of the never-dried microsphere.

3.4.4 Release profiles: A comparison of non-swelling and swelling models

Release profiles were fitted to the model of exponential decay between 5-120 minutes and analysed. The total amount of the loaded drug was taken from the maximum y-offset value at any used pH for each ACB (Figure 3.26). This value was used to relate the release profiles (Figure 3.28). At pH 7.4 ACB60 released less drugs than it did at pH 1.2 (Figure 3.26). Swelling at this pH is notably higher than, for example, at pH 3.6 (Table 3.3) and since the solubility of the ranitidine hydrochloride increases at elevated pH environment (Mirmehrabi et al., 2004), it is possible that some ionic interactions between anionic cellulose and cationic drug inhibited the complete release.

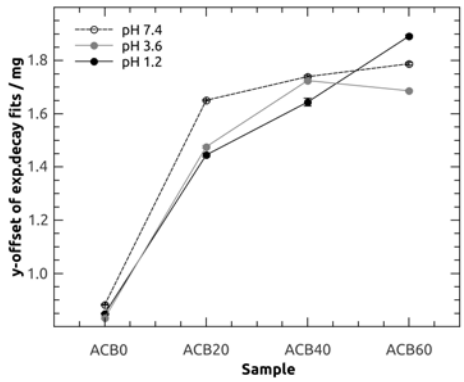

Figure 3.26: Released amount of ranitidine hydrochloride per one ACB at different pH environment.

At pH 1.2 ranitidine hydrochloride and ACBs were in protonated form, so the e-folding release times were short (Figure 3.27). Since the cellulose matrix did not swell at this pH, diffusion of the solubilised drug took place through the hornified channels. The increase in times of ACB40-60 could be explained by higher loading capacity and more intense hornification due to higher porosity and water content in never-dried microspheres.

At pH 3.6 release times were increased because the pH was near the pK_a of ranitidine hydrochloride and oxidised ACBs, so both were partially in ionic form. The swelling at this pH was higher than at pH 1.2 for oxidised ACBs, but still clearly lower than at pH 7.4 (Table 3.3). The drug and the matrix are in ionic form at pH 7.4 and this decreased the release times, however, the solubility of the ranitidine hydrochloride increases at elevated pH.

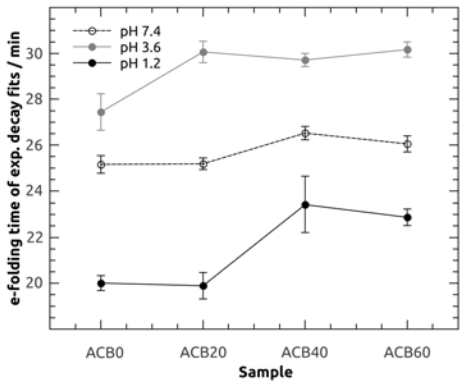

Figure 3.27: Release times (e-fold) of ranitidine hydrochloride from ACBs at various pH environments.

Release profiles were nearly independent of the oxidation temperature and the pH of the environment (Figure 3.28). Fit to the model of exponential decay was high ($R^2 \geq 0.998$) and the similarity of the curves indicates that the pores were already so open in dried microspheres that the highly soluble drug could dissolve without additional opening of the oxidised cellulose matrix.

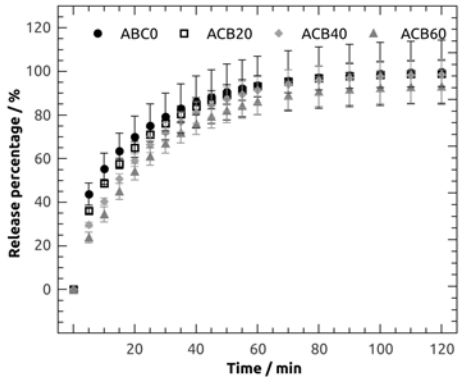

Figure 3.28: Cumulative drug release rates of ranitidine hydrochloride from ACBs at pH 7.4.

Fit to the models of swelling and static spheres

Baker-Lonsdale model Equation 2.5 is valid for dispersed drug systems (Baker and Lonsdale, 1974). This was used since the drug was incorporated in microspheres by filling the pores with drug solution and then entrapping them by drying at room temperature. The loading mechanism for dissolved

Table 3.4: Release constants and correlation coefficients of fits to Baker-Lonsdale's and Ritger-Peppas's models at linear region 5-30 min.

Sample	pH	Baker-Lonsdale		Ritger-Peppas, n=0.43	
		k^*	R^2	k^*	R^2
ACB0	1.2	6.1±0.2	0.9983	15.5±1.2	0.9794
	3.6	4.6±0.2	0.9977	15.3±0.4	0.9984
	7.4	5.7±0.1	0.9996	17.5±0.7	0.9941
ACB20	1.2	4.5±0.1	0.9995	1.8±0.3	0.9445
	3.6	3.3±0.1	0.9999	11.5±0.1	0.9998
	7.4	5.4±0.1	0.9995	17.5±0.3	0.9991
ACB40	1.2	4.7±0.2	0.9926	1.8±0.3	0.9313
	3.6	4.5±0.1	0.9994	14.9±0.2	0.9994
	7.4	5.0±0.2	0.9934	16.7±0.5	0.9974
ACB60	1.2	5.9±0.1	0.9989	2.3±0.3	0.9428
	3.6	3.3±0.1	0.9998	11.4±0.1	0.9998
	7.4	4.2±0.2	0.9914	14.7±0.6	0.9948

* $\times 10^{-3}$

drug systems would require sorption on to the surface.

Release profiles were fitted to the model of non-swelling monolithic spheres (Equation 2.5). The model fits with high correlation at a linear region of 5-30 minutes early time release profile. Any significant relation was not observed between swellability and correlation coefficients (Table 3.4). Baker and Lonsdale (1974) stated that the higher loading of the dispersed drug yields to lower release at a given time. This was seen at pH 7.4 but not at lower pH values (Table 3.4). The lowest release constants were computed for pH 3.6 environment, which is consistent with fits to the exponential decay model (Figure 3.27).

Ritger-Peppas's model A model for swelling spheres (Equation 2.6, n=0.43) was compared with a non-swelling model. The correlation coefficient of the swelling model by Ritger-Peppas (1987) was poor at pH 1.2 for all the ACBs ($R^2 \leq 0.97$), as expected since the microspheres did not swell (Table 3.3).

However, correlations were higher for ACB0 at other pH values even though ACB0 did not swell at these environments either.

As well as the similar or poorer correlation coefficients compared to the non-swelling mode by Baker and Lonsdale, release constants at oH values 3.6 and 7.4 were not consistent with observations; higher release constants of ACB20-60 at pH 7.4 indicate notably faster release than at pH 3.6, which was not confirmed by the model of exponential decay nor observations. Release profiles were almost independent of the microsphere type and pH of the environment.

Ritger-Peppas's model for swelling spheres did not give realistic results, and some relatively high correlations were even gained. Spheres wee swelling in physiological pH 3.6-7.4 but since the drug maintains the open pores during the drying of the microspheres, a highly soluble drug dissolves and diffuses through the open pores before swelling affects the release kinetics.

3.5 Paper V: Discussion. Potential applications

Cellulose is a nontoxic compound which is approved in pharmaceutical and food applications in Europe under code E460. Many of its derivatives, such as methyl, ethyl, hydroxypropyl, hydroxypropylmethyl, methylethyl and carboxymethyl cellulose (MC, EC, HPC, HPMC, MEC, CMC) are approved under codes E461-466 and used as a thickening agents and stabilisers in food products and disintegrants in pharmaceuticals. Due to structural properties of the backbone and the versatility of its various derivatives, cellulose is widely used in applications. This section is an overview of the possible ways that cellulose microspheres can be utilised in applications.

3.5.1 Chromatographic columns

Their spherical shape allows the dense packing of the cellulose microspheres in columns. With a narrow size distribution — ideally the ratio of radii ~0.41 and above — it is possible to achieve ~0.74 packing density. They also have smaller flow resistance than powders and more mechanical strength against deformations than, for example, cross-linked dextrans (Kaster et al., 1993).

Due to the high and adjustable porosity of the cellulose microspheres they can

be used in size-exclusion chromatography (Oliveira and Glasser, 1996). SEC requires that the interactions between the stationary phase and separating molecules are minimised, so that separation would only occur according to the hydrodynamic radii of the components. Interactions between hydroxyl groups of the cellulose and separating molecules could be minimised by silylation of the cellulose (Xiong et al., 2005).

In affinity chromatography the separation is created by delaying or binding some molecules by adsorption in the stationary phase while others are elueted first. Affinity chromatography can be specific, if, for example, dye-ligands are used for specific binding sites (Figure 3.29). Unspecific affinity is based on ionic or hydrophobic/-philic interactions. For example, higher affinity of multivalent heavy metal cations towards anionic groups of oxidised cellulose beads (Hirota et al., 2009) could be used in water purification. In the case of total binding, the adsorbed molecules can be released afterwards by adjusting the pH or salt concentration (Sakata et al., 2006), or introducing the more fitting competing free counterparts.

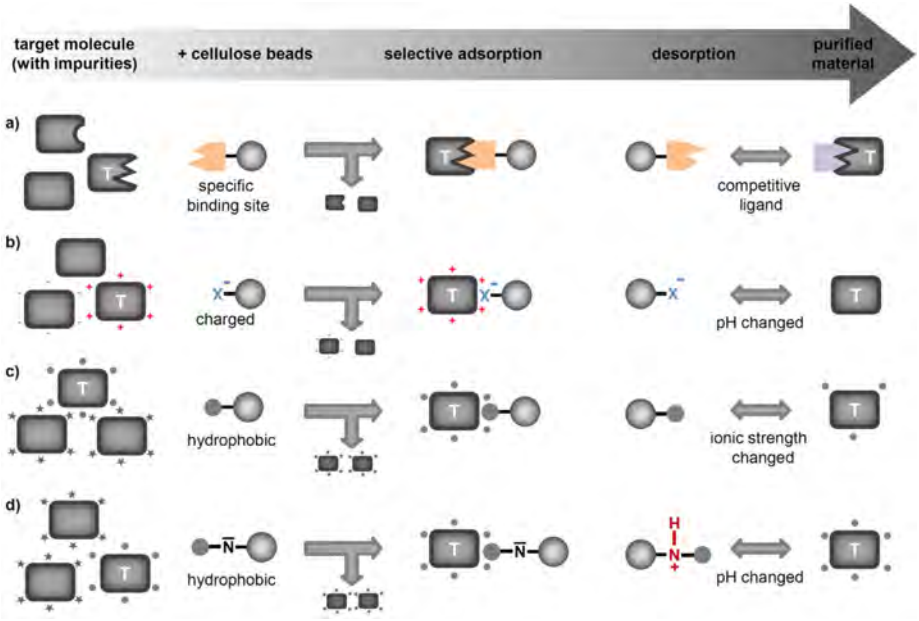

Figure 3.29: Affinity chromatographic techniques. Specific ligand-dye (a) and unspecific ion exchange (b), hydrophobic (c) and hydrophobic charge induction chromatographies.

3.5.2 Anchoring and immobilisation

Functionalised cellulose microspheres can be used as a solid-state supports. Their closed structure can protect often complex and perhaps expensive enzymes and proteins from contaminations, and undesired reactions with laboratory glassware, making it possible to collect and re-use the enzyme. They also provide an isolated space where the reactions can occur in higher yields (Guillier et al., 2000). Anchoring the reagent to the solid-state support can assist the reaction to the intermediate state (Figure 3.30) and cleaving off the final product simultaneously regenerates the solid support (De Luca et al., 2003).

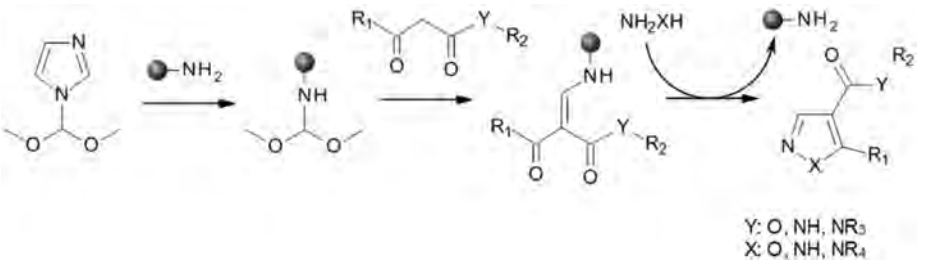

Figure 3.30: Synthesis of pyrazoles and isoxazoles using cellulose beads as a solid-state support for anchoring the reagent. Adapted from De Luca et al. (2003).

Immobilisation is used when the bound component has a specific property, such as a value or a way to interact with the environment. To separate it from the derivatisation, immobilised component could also perform and exist without the substrate, the cellulose microsphere, but the immobilisation enhances its property to act in the desired manner. Weber et al. (2005) demonstrated four times higher binding capacities of tumour necrosis factor-α when the antibodies were not randomly oriented but immobilised in a certain orientation on the cellulose microsphere (Figure 3.31).

3.5.3 Drug delivery

Uniform distribution of drugs in carrier capsules, pellets or tablets is crucial for several reasons; the release profile has to be steady or at least predictable, dosing repeatable, and high or low local release dosages avoidable. Cellulose microspheres, prepared by dissolution and coagulation via gelation phase, have uniform internal structure and shape. When the drug is loaded in the

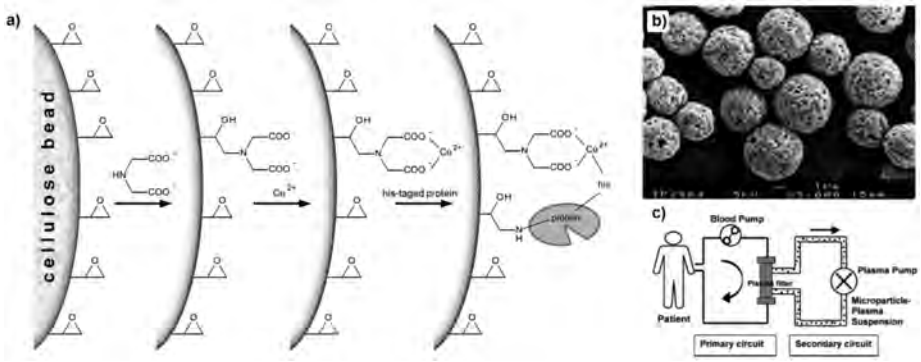

Figure 3.31: Preparation of (a) cellulose microsphere surface functionalised with aligned (his)-tagged antibody, (b) SEM image of microspheres and (c) schematic presentation of two-circuit system for blood plasma purification. Adapted from Weber et al. (2005).

microsphere using the dissolution method (microsphere immersed in drug solution, loading driven by diffusion) an equilibrium state is achieved and distribution is even.

As we demonstrated in Paper IV, due to the dense gel-matrix inside the microspheres the drug is in an amorphous form after drying. This could enhance the solubility of poorly soluble drugs. Adding anionic charge might create the better solubility of these drugs by offering less attractive moiety for the ionic counterpart. Prazosin hydrochloride is a poorly soluble drug (25 mg dm^3 at pH 6.8) but when it was coupled to anionic cellulose phosphate it dissolved rapidly in buffer solution (Figure 3.32).

Enteric administration of APIs (active pharmaceutical ingredients) can be easily carried out with millimetre-sized microspheres. Designing the matrix (see Section 1.4 Controlled release systems) so that the APIs are released in certain part of the gastrointestinal track at a certain rate defines other components and/or derivatives of the microsphere. Matrices could have, for example, higher amounts of swelling agents, so that in certain environments the structure would disintegrate due to too extensive swelling and/or dissolution. This could be initiated by a change in pH, temperature or even magnetic field (Figure 1.4). Binary systems could be utilised in microspheres by derivatising only the surface with hydrophobic groups and physically creating a small holes in this layer (Figure 1.4G).

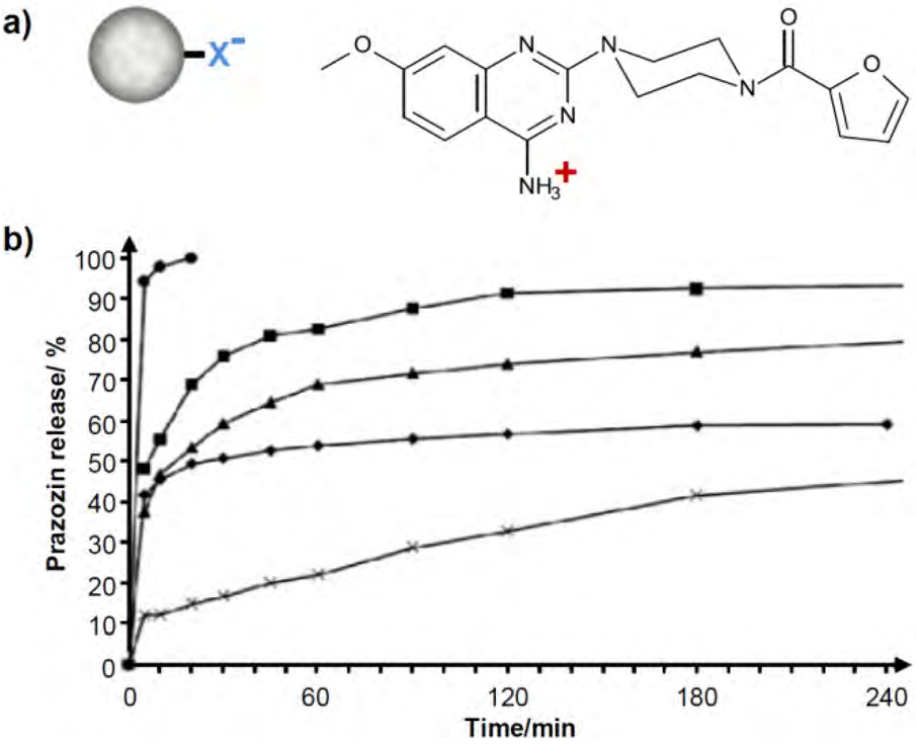

Figure 3.32: a) Schematic illustration of anionic cellulose microsphere and anionic prazosin; b) Prazosin release into the buffer solution from cellulose phosphate (-●-), carboxymethyl (ethanol dried, -■-), and carboxymethyl microspheres (water dried, -▲-) and powder tablet (-♦-) and pure prazosin hydrochloride (-×-). Adapted from Volkert et al. (2009).

4 Concluding remarks

The challenge of dissolving cellulose in water-based solvent was met with a new type of pretreatment. Pulp was immersed in ethanol-acid solution for different times and temperatures, and the solubility of the cellulosic fibre was studied. Clear solutions were gained without undissolved fragments, even though solutions with higher concentrations were not so-called true solutions and formed aggregates between cellulose molecules.

The effect of coagulation kinetics and cellulose concentration on the properties of cellulose microspheres was studied after the dissolution. Highly alkaline cellulose dope was extruded through a syringe into an acid of different concentrations and temperatures. Variations in coagulation kinetics produced microspheres with different pore size distributions and specific surface areas, whereas total porosity remained high in all samples. Variations in measured properties had no effect, for example, on the release profiles of the various active pharmaceutical ingredients, but the solubility of each drug was the dominant parameter.

Microspheres were oxidised with the well-known Anelli's oxidation system with modifications, commonly known as TEMPO-mediated oxidation. This introduced a high anionic charge on microspheres with even distribution. Oxidised microspheres demonstrated enhanced water-retention, swelling at higher pH environments, and porosity. The opening of the small micro- and mesopores made it possible to load more than twice as much drug in microspheres than in non-oxidised microspheres. Drug release profiles of the highly soluble model drug were still noted to be very similar regardless of the oxidation level or the pH of the environment, indicating an open pore network of the drug loaded dry microsphere.

Further analysis showed that the swelling of the anionic microspheres at any pH does not play a role in release profiles. Fit to the model of non-swelling spheres (Baker-Lonsdale) was clearly better and was in agreement with observations than the fit to the model of swelling spheres (Ritger-Peppas).

Solid-state analysis revealed that the model drug, ranitidine hydrochloride,

was in amorphous form after loading in microspheres. This is one of the challenges in the pharmaceutical industry; crystallisation of poorly soluble drugs and their rapid release. Amorphicity of the drugs and the high swelling capability of the oxidised microspheres could be utilised in the delivery of these pharmaceutical ingredients.

Another clear benefit of microspheres is their even mass distribution and easy loading. Since the droplet formation of cellulose dope is very even, each sphere contains an exact amount of cellulose and volume. Loading degree is constant since all the spheres are loaded in the same drug solution of known concentration. Due to the large size of spheres, the personalised dosing of drugs would be simple.

5 Acknowledgements

I am intensely grateful to my supervisor Professor Pedro Fardim, for this opportunity to work in comfort at FCT all these years. The feeling of security made it possible to let my mind fly and to grow as a researcher and as a person. Thank you for your patience, sincere trust and support.

I am thankful to TEKES for financing the FuBio project and to the Finnish Bioeconony Cluster (FiBiC) for coordinating it. Thank you for the opportunity to take part in numerous domestic and international events. These are important lessons for us, and opportunities for networking.

I am thankful to all the members at FCT for making the environment colourful and adventurous. It has been a pleasure to do research with all of you. I would also like to thank the staff of 3PK and PAF for their help and cooperation. This work could not have been done without you. Thanks also to our partners at Pharmaceutical Sciences; Professor Niklas Sandler, Doctors Ruzica Kolakovic and Natalja Genina, and Emrah Yildir. Half of my papers are done with you.

Thank you Agneta Hermansson, without you I would not have travelled anywhere, had lab notebooks nor pens, and my coffee breaks would have been much more dull. Jan Gustafsson, tack ska du ha för översatte mina texter på svenska. You also provided me with education that I should already have had when I came to FCT. Post-docs Anne Kotiaho and Martin Gericke, a sincere thank you for your wisdom and instructions. Colleagues Elina Heikkilä and Carl Lange, thank you for endless philosophical and practical conversations about life and science, wondering how to be an academic and a human, at the same time.

At last, I would like to thank my friends along this long journey, old and new. You know who you are. You have been understanding. Your presence has been the source of my strength and so needed during the hard times. My family, my parents and grandparents, your support has been most appreciated. I cannot promise that I will get a real job after this, but I promise to go where my heart takes me and where my mind is peaceful. Sara, thank you for your love and smiles, they mean the world to me.

Bibliography

Adel, A. M., El–Wahab, Z. H. A., Ibrahim, A. A., and Al–Shemy, M. T. (2010). Characterization of microcrystalline cellulose prepared from lignocellulosic materials. Part I. Acid catalyzed hydrolysis. *Bioresource Technology*, 101(12):4446–4455.

Anelli, L. P., Biffi, C., Montanari, F., and Quici, S. (1987). Fast and selective oxidation of primary alcohols to aldehydes or to carboxylic acids and of secondary alcohols to ketones mediated by oxoammonium salts under two-phase conditions. *The Journal of Organic Chemistry*, 52:2559–2562.

Arifin, D. Y., Lee, L. Y., and Wang, C.-H. (2006). Mathematical modeling and simulation of drug release from microspheres: Implications to drug delivery systems. *Advanced Drug Delivery Reviews*, 58:1274–1325.

Baker, R. and Lonsdale, H. (1974). Advances in experimental medicine and biology. Vol. 47 of *Controlled Release of Biologically Active Agents*, Chapter: Controlled release: Mechanisms and rates, pages 15–71. Plenum Press, New York.

Biganska, O., Navard, P., and Bédué, O. (2002). Crystallisation of cellulose/N-methylmorpholine-N-oxide hydrate solutions. *Polymer*, 43:6139–6145.

Brown, R. M. (1985). Cellulose microfibril assembly and orientation: Recent developments. *Journal of Cell Science*, 1985:13–32.

Brown Jr, R. M., Saxena, I. M., and Kudlicka, K. (1996). Cellulose biosynthesis in higher plants. *Trends in Plant Science*, 1(5):149–156.

Brunauer, S., Emmett, P. H., and Teller, E. (1938). Adsorption of gases in multimolecular layers. *Journal of the American Chemical Society*, 60(2):309–319.

Budd, J. and Herrington, T. M. (1989). Surface charge and surface area of cellulose fibres. *Colloids and Surfaces*, 36(3):273–288.

Cai, J. and Zhang, L. (2005). Rapid dissolution of cellulose in lioh/urea and naoh/urea aqueous solutions. *Macromolecular Bioscience*, 5(6):539–548.

Capello, C., Fischer, U., and Hungerbuhler, K. (2007). What is a green solvent? a comprehensive framework for the environmental assessment of solvents. *Green Chemistry*, 9(9):927–934.

Carr, J. and Walker, D. (1968). An annular shear cell for granular materials. *Powder Technology*, 1(6):369–373.

Carr, R. (1965). Evaluating flow properties of solids. *Chemical Engineering*, 72:163–168.

Carrillo, F., Lis, M., Colom, X., López-Mesas, M., and Valldeperas, J. (2005). Effect of alkali pretreatment on cellulase hydrolysis of wheat straw: Kinetic study. *Process Biochemistry*, 40(10):3360–3364.

Chen, P., Cho, S., and Jin, H.-J. (2010). Modification and applications of bacterial celluloses in polymer science. *Macromolecular Research*, 18(4):309–320.

Chieng, N., Rehder, S., Saville, D., Rades, T., and Aaltonen, J. (2009). Quantitative solid-state analysis of three solid forms of ranitidine hydrochloride in ternary mixtures using raman spectroscopy and x-ray powder diffraction. *Journal of Pharmaceutical and Biomedical Analysis*, 49:18–25.

Conn, H. J. (1953). *Biological stains; a handbook on the nature and uses of the dyes employed in the biological laboratory*. The Williams & Wilkins Company, Baltimore, Maryland, 6th edition.

Cuissinat, C. and Navard, P. (2006a). Swelling and dissolution of cellulose, part 1: Free floating cotton and wood fibres in N-methylmorpholine-N-oxide-water mixtures. *Macromolecular Symposia*, 244:1–18.

Cuissinat, C. and Navard, P. (2006b). Swelling and dissolution of cellulose, part II: Free floating cotton and wood fibres in NaOH-water-additives systems. *Macromolecular Symposia*, 244:19–30.

Cuissinat, C. and Navard, P. (2008). Swelling and dissolution of cellulose, part iii: Plant fibres in aqueous systems. *Cellulose*, 15:67–74.

Dahiya, J. and Rana, S. (2004). Thermal degradation and morphological studies on cotton cellulose modified with various arylphosphorodichloridites. *Polymer International*, 53(7):995–1002.

De Luca, L., Giacomelli, G., Porcheddu, A., Salaris, M., and Taddei, M. (2003). Cellulose beads: A new versatile solid support for microwave- assisted synthesis. Preparation of pyrazole and isoxazole libraries. *Journal of Combinatorial Chemistry*, 5:465–471.

de Nooy, A. E., Besemer, A. C., and van Bekkum, H. (1995). Highly selective nitroxyl radical-mediated oxidation of primary alcohol groups in water-soluble glucans. *Carbohydrate Research*, 269:89–98.

Domsjö (2007). Specification Domsjö Cellulose. http://www.domsjoe.com - Produkter - Specialcellulosa - Produktinformation Domsjö Cellulose. Accessed 10 November 2010.

Du, K.-F., Yan, M., Wang, Q.-Y., and Song, H. (2010). Preparation and characterization of novel macroporous cellulose beads regenerated from ionic liquid for fast chromatography. *Journal of Chromatography A*, 1217(8):1298–1304.

Ettenauer, M., Loth, F., Thümmler, K., Fischer, S., Weber, V., and Falkenhagen, D. (2011). Characterization and functionalization of cellulose microbeads for extracorporeal blood purification. *Cellulose*, 18:1257–1263.

Fardim, P. and Holmbom, B. (2003). Fast determination of anionic groups in different pulp fibers by methylene blue sorption. *Tappi*, 2:28–32.

Fardim, P., Holmbom, B., Ivaska, A., Karhu, J., Mortha, G., and Laine, J. (2002). Critical comparison and validation of methods for determination of anionic groups in pulp fibres. *Nordic Pulp and Paper Research Journal*, 17:346–351.

Fink, H.-P., Weigel, P., Purz, H., and Ganster, J. (2001). Structure formation of regenerated cellulose materials from NMMO-solutions. *Progress in Polymer Science*, 26(9):1473–1524.

Gavillon, R. and Budtova, T. (2008). Aerocellulose: New highly porous cellulose prepared from cellulose-NaOH aqueous solutions. *Biomacromolecules*, 9(1):269–277.

Gericke, M., Fardim, P., and Heinze, T. (2012). Ionic liquids — promising but challenging solvents for homogeneous derivatization of cellulose. *Molecules*, 17(6):7458–7502.

Gericke, M., Trygg, J., and Fardim, P. (2013). Functional cellulose beads: Preparation, characterization, and applications. *Chemical Reviews*, 113:4812–4836.

Grznárová, G., Yu, S., Štefuca, V., and Polakovič, M. (2005). Quantitative characterization of pore structure of cellulose gels with or without bound protein ligand. *Journal of Chromatography A*, 1092(1):107–113.

Guillier, F., Orain, D., and Bradley, M. (2000). Linkers and cleavage strategies in solid-phase organic synthesis and combinatorial chemistry. *Chemical Reviews*, 100(6):2091–2158.

Heinze, T., Liebert, T., and Koschella, A. (2006). *Esterification of Polysaccharides*. Springer, Berlin Heidelberg.

Heinze, T., Schwikal, K., and Barthel, S. (2005). Ionic liquids as reaction medium in cellulose functionalization. *Macromolecular Bioscience*, 5(6):520–525.

Hendriks, A. and Zeeman, G. (2009). Pretreatments to enhance the digestibility of lignocellulosic biomass. *Bioresource Technology*, 100(1):10–18.

Hirota, M., Tamura, N., Saito, T., and Isogai, A. (2009). Oxidation of regenerated cellulose with $NaClO_2$ catalyzed by TEMPO and NaClO under acid-neutral conditions. *Carbohydrate Polymers*, 78:330–335.

Immergut, E., Schurz, J., and Mark, H. (1953). Viskositätszahl-molekulargewichts-beziehung für cellulose und untersuchungen von nitrocellulose in verschiedenen lösungsmitteln. *Monatshefte für Chemie*, 84:219–249.

Isogai, A. and Atalla, R. H. (1998). Dissolution of cellulose in aqueous NaOH solutions. *Cellulose*, 5:309–319.

Isogai, A., Saito, T., and Fukuzumi, H. (2011). TEMPO-oxidized cellulose nanofibers. *Nanoscale*, 3:71–85.

Jensen, V., editor (1977). *Puukemia*. Suomen Paperi-insinöörien Yhdistyksen oppi- ja käsikirja I. Teknillisten Tieteiden Akatemia, 2nd edition.

Jin, H., Zha, C., and Gu, L. (2007). Direct dissolution of cellulose in NaOH/thiourea/urea aqueous solution. *Carbohydrate Research*, 342(6):851–858.

Jonas, R. and Farah, L. F. (1998). Production and application of microbial cellulose. *Polymer Degradation and Stability*, 59(1–3):101–106.

Jonoobi, M., Niska, K. O., Harun, J., and Misra, M. (2009). Chemical composition, crystallinity, and thermal degradation of bleached and unbleached kenaf bast (hibiscus cannabinus) pulp and nanofibers. *BioResources*, 4(2):626–639.

Kamide, K., Okajima, K., and Kowsaka, K. (1992). Dissolution of natural cellulose into aqueous alkali solution: Role of super-molecular structure of cellulose. *Polymer Journal*, 24(1):71–86.

Kaster, J. A., de Oliveira, W., Glasser, W. G., and Velander, W. H. (1993). Optimization of pressure-flow limits, strength, intraparticle transport and dynamic capacity by hydrogel solids content and bead size in cellulose immunosorbents. *Journal of Chromatography A*, 648:79–90.

Kim, S. and Holtzapple, M. T. (2006). Delignification kinetics of corn stover in lime pretreatment. *Bioresource Technology*, 97(5):778–785.

King, A. W. T., Asikkala, J., Mutikainen, I., Järvi, P., and Kilpeläinen, I. (2011). Distillable acid–base conjugate ionic liquids for cellulose dissolution and processing. *Angewandte Chemie*, 123(28):6425–6429.

Klemm, D., Heublein, B., Fink, H.-P., and Bohn, A. (2005). Cellulose: Fascinating biopolymer and sustainable raw material. *Angewandte Chemie (Int.Ed)*, 44(22):3358–3393.

Klemm, D., Philipp, B., Heinze, T., Heinze, U., and Wagenknecht, W. (1998). *Comprehensive Cellulose Chemistry: Functionalization of Cellulose*. Wiley-VCH, Weinheim.

Kolpak, F. J. and Blackwell, J. (1976). Determination of the structure of cellulose II. *Macromolecules*, 9(2):273–278.

Konkin, A., Wendler, F., Meister, F., Roth, H.-K., Aganov, A., and Ambacher, O. (2008). N-Methylmorpholine-N-oxide ring cleavage registration by ESR under heating conditions of the Lyocell process. *Spectrochimica Acta Part A*, 69(3):1053–1055.

Kosan, B., Michels, C., and Meister, F. (2008). Dissolution and forming of cellulose with ionic liquids. *Cellulose*, 15(1):59–66.

Krässig, H. and Kitchen, W. (1961). Factors influencing tensile properties of cellulose fibers. *Journal of Polymer Science*, 51(155):123–172.

Kumar, P., Barrett, D. M., Delwiche, M. J., and Stroeve, P. (2009). Methods for pretreatment of lignocellulosic biomass for efficient hydrolysis and biofuel production. *Industrial & Engineering Chemistry Research*, 48(8):3713–3729.

Lagus, H., Sarlomo-Rikala, M., Böhling, T., and Vuola, J. (2013). Prospective study on burns treated with Integra ®, a cellulose sponge and split thickness skin graft: Comparative clinical and histological study - Randomized controlled trial. *Burns*, 39(8):1577–1587.

Langer, R. (1990). New methods of drug delivery. *Science (New York, N.Y.)*, 249(4976):1527–1533.

Langer, R. (1993). Polymer-controlled drug delivery systems. *Accounts of Chemical Research*, 26(10):537–542.

Larkin, P. (2011). *Infrared and Raman Spectroscopy*. Elsevier, Oxford.

Leong, K. and Langer, R. (1988). Polymeric controlled drug delivery. *Advanced Drug Delivery Reviews*, 1(3):199–233. Immunoliposomes in Vivo.

Li, J., Gellerstedt, G., and Toven, K. (2009). Steam explosion lignins; their extraction, structure and potential as feedstock for biodiesel and chemicals. *Bioresource Technology*, 100(9):2556–2561.

Liebert, T. (2010). *Cellulose Solvents – Remarkable History, Bright Future*, Vol. 1033 of *ACS Symposium Series*, Chapter: 1, pages 3–54. American Chemical Society, Washington, USA.

Liu, W., Budtova, T., and Navard, P. (2011). Influence of ZnO on the properties of dilute and semi-dilute cellulose-NaOH-water solutions. *Cellulose*, 18:911–920.

Lonkar, S.S., K. G. K. J. and Kale, M. (2011). Dyes and chemicals used in biomaterial study as stains for invertebrates. *International Journal of Chemistry Research*, 2:22–25.

Loth, F., Schaaf, E., Weigel, P., Fink, H. P., and Gensrich, J. (2003). *WO Patent App. PCT/EP2003/004,879*, Munich, Germany. European Patent Office.

Lu, X., Zhang, Y., Yang, J., and Liang, Y. (2007). Enzymatic hydrolysis of corn stover after pretreatment with dilute sulfuric acid. *Chemical Engineering & Technology*, 30(7):938–944.

Lue, A., Zhang, L., and Ruan, D. (2007). Inclusion complex formation of cellulose in NaOH–thiourea aqueous system at low temperature. *Macromolecular Chemistry and Physics*, 208(21):2359–2366.

Ma, Y., Loyns, C., Price, P., and Chechik, V. (2011). Thermal decay of TEMPO in acidic media via an N-oxoammonium salt intermediate. *Organic & Biomolecular Chemistry*, 9:5573–5578.

McCormick, C. L., Callais, P. A., and Hutchinson, B. H. (1985). Solution studies of cellulose in lithium chloride and N,N-dimethylacetamide. *Macromolecules*, 18:2394–2401.

McGraw-Hill (2003). *McGraw-Hill Dictionary of Chemistry*. McGraw-Hill, USA, 2nd edition.

McMillan, J. D. (1994). 15. Pretreatment of Lignocellulosic Biomass. In Himmel, M. E., Baker, J. O., and Overend, R. P., editors, *Enzymatic Conversion of Biomass for Fuels Production*, Vol. 566 of *ACS Symposium Series*, pages 292–324, Washington, USA. American Chemical Society.

Merriam-Webster (2014). Online dictionary. Keywords: Coagulation / regeneration / gelation / sponge. Encyclopaedia Britannica. Accessed in September 2014.

Mirmehrabi, M., Rohani, S., Murthy, K., and Radatus, B. (2004). Solubility, dissolution rate and phase transition studies of ranitidine hydrochloride tautomeric forms. *International Journal of Pharmaceutics*, 282:73–85.

Miyamoto, T., Takahashi, S.-i., Ito, H., Inagaki, H., and Noishiki, Y. (1989). Tissue biocompatibility of cellulose and its derivatives. *Journal of Biomedical Materials Research*, 23(1):125–133.

Moigne, N. L., Spinu, M., Heinze, T., and Navard, P. (2010). Restricted dissolution and derivatization capacities of cellulose fibres under uniaxial elongational stress. *Polymer*, 51:447–453.

Mosier, N., Wyman, C., Dale, B., Elander, R., Lee, Y., Holtzapple, M., and Ladisch, M. (2005). Features of promising technologies for pretreatment of lignocellulosic biomass. *Bioresource Technology*, 96(6):673–686.

Navard, P., Cuissinat, C., and Heinze, T. (2008). Swelling and dissolution of cellulose. Part IV: Free floating cotton and wood fibres in ionic liquids. *Carbohydrate Polymers*, 72:590–596.

Nichols, G., Byard, S., Bloxham, M. J., Botterill, J., Dawson, N. J., Dennis, A., Diart, V., North, N. C., and Sherwood, J. D. (2002). A review of the terms agglomerate and aggregate with a recommendation for nomenclature used in powder and particle characterization. *Journal of Pharmaceutical Sciences*, 91(10):2103–2109.

Niklas, K. (1992). *Plant Biomechanics: An Engineering Approach to Plant Form and Function*. University of Chicago Press, USA.

Nobles, D. R., Romanovicz, D. K., and Brown, R. M. (2001). Cellulose in cyanobacteria. Origin of vascular plant cellulose synthase? *Plant Physiology*, 127(2):529–542.

Oliveira, W. D. and Glasser, W. G. (1996). Hydrogels from polysaccharides. I. Cellulose beads for chromatographic support. *Journal of Applied Polymer Science*, 60(1):63–73.

Origin Software. Origin software, version 7.0. OriginLab Corporation, 2002, Northampton, MA, USA.

Palmqvist, E. and Hahn-Hägerdal, B. (2000). Fermentation of lignocellulosic hydrolysates. II: inhibitors and mechanisms of inhibition. *Bioresource Technology*, 74(1):25–33.

Pekala, R., Alviso, C., and LeMay, J. (1990). Organic aerogels: microstructural dependence of mechanical properties in compression. *Journal of Non-Crystalline Solids*, 125(1-2):67–75.

Perpetuo, G., Galico, D., Fugita, R., Castro, R., Eusebio, M., Treu-Filho, O., Silva, A., and Bannach, G. (2013). Thermal behavior of some antihistamines. *Journal of Thermal Analysis and Calorimetry*, 111:2019–2028.

Pinnow, M., Fink, H.-P., Fanter, C., and Kunze, J. (2008). Characterization of highly porous materials from cellulose carbamate. *Macromolecular Symposia*, 262(1):129–139.

Qi, H., Chang, C., and Zhang, L. (2008). Effects of temperature and molecular weight on dissolution of cellulose in NaOH/urea aqueous solution. *Cellulose*, 15:779–787.

Qin, X., Lu, A., Cai, J., and Zhang, L. (2013). Stability of inclusion complex formed by cellulose in NaOH/urea aqueous solution at low temperature. *Carbohydrate Polymers*, 92(2):1315–1320.

Qtiplot (2011). Version 0.9. http://soft.proindependent.com/qtiplot.html. Accessed 30.08.2013.

Quesada, J., Rubio, M., and Gomez, D. (1999). Ozonation of lignin rich solid fractions from corn stalks. *Journal of Wood Chemistry and Technology*, 19(1-2):115–137.

Ritger, P. L. and Peppas, N. A. (1987). A simple equation for description of solute release I. Fickian and non-fickian release from non-swellable devices in the form of slabs, spheres, cylinders or discs. *Journal of Controlled Release*, 5:23–36.

Roberts, E., Saxena, I., and Brown Jr, R. (1989). *Cellulose and Wood: Chemistry and Technology*, Chapter: Biosynthesis of cellulose II in Acetobacter Xylinum, pages 689–704. Wiley & Sons, New York.

Rosenau, T., Potthast, A., Sixta, H., and Kosma, P. (2001). The chemistry of side reactions and byproduct formation in the system NMMO/cellulose (Lyocell process). *Progress in Polymer Science*, 26(9):1763–1837.

Rosenberg, P., Suominen, I., Rom, M., Janicki, J., and Fardim, P. (2007). Tailored cellulose beads for novel applications. *Cellulose Chemistry and Technology*, 41:243–254.

Ross, P., Mayer, R., and Benziman, M. (1991). Cellulose biosynthesis and function in bacteria. *Microbiological Reviews*, 55(1):35–58.

Roy, C., Budtova, T., and Navard, P. (2003). Rheological properties and gelation of aqueous cellulose-NaOH solutions. *Biomacromolecules*, 4:256–264.

Sakata, M., Nakayama, M., Yanagi, K., Sasaki, M., Kunitake, M., and Hirayama, C. (2006). Selective removal of dna from bioproducts by polycation-immobilized cellulose beads. *Journal of Liquid Chromatography & Related Technologies*, 29(17):2499–2512.

Scheffer, T. C. (1966). Natural resistance of wood to microbial deterioration. *Annual Review of Phytopathology*, 4(1):147–168.

Schenzel, K. and Fischer, S. (2001). NIR FT Raman Spectroscopy - Rapid analytical tool for detecting the transformation of cellulose polymorphs. *Cellulose*, 8:49–57.

Schilling, J., Tewalt, J., and Duncan, S. (2009). Synergy between pretreatment lignocellulose modifications and saccharification efficiency in two brown rot fungal systems. *Applied Microbiology and Biotechnology*, 84:465–475. 10.1007/s00253-009-1979-7.

Schindelin, J. (2008). Fiji Is Just ImageJ (batteries included). version 1.44. ImageJ User and Developer Conference.

Sen, V. D. and Golubev, V. A. (2009). Kinetics and mechanism for acid-catalyzed disproportionation of 2,2,6,6-tetramethylpiperidine-1-oxyl. *Journal of Physical Organic Chemistry*, 22(2):138–143.

Sescousse, R., Gavillon, R., and Budtova, T. (2011a). Aerocellulose from cellulose-ionic liquid solutions: Preparation, properties and comparison with cellulose-naoh and cellulose-nmmo routes. *Carbohydrate Polymers*, 83(4):1766–1774.

Sescousse, R., Gavillon, R., and Budtova, T. (2011b). Wet and dry highly porous cellulose beads from cellulose-NaOH-water solutions: Influence of the preparation conditions on beads shape and encapsulation of inorganic particles. *Journal of Materials Science*, 46:759–765.

Stone, J. and Scallan, A. (1967). The effect of component removal upon the porous structure of the cell wall of wood. II. Swelling in water and the fiber saturation point. *Tappi*, 50:496–501.

Stone, J. and Scallan, A. (1968). A structural model for the cell wall of water-swollen wood pulp fibres based on their accessibility to macromolecules. *Cellulose Chemistry and Technology*, 2:343–358.

Svensson, A., Larsson, P. T., Salazar-Alvarez, G., and Wågberg, L. (2013). Preparation of dry ultra-porous cellulosic fibres: Characterization and possible initial uses. *Carbohydrate Polymers*, 92(1):775–783.

Swatloski, R. P., Spear, S. K., Holbrey, J. D., and Roger, R. D. (2002). Dissolution of cellose with ionic liquids. *Journal of American Chemical Society*, 124:4974–4975.

Tassinari, T., Macy, C., Spano, L., and Ryu, D. D. Y. (1980). Energy requirements and process design considerations in compression-milling pretreatment of cellulosic wastes for enzymatic hydrolysis. *Biotechnology and Bioengineering*, 22(8):1689–1705.

Thümmler, K., Fischer, S., Feldner, A., Weber, V., Ettenauer, M., Loth, F., and Falkenhagen, D. (2011). Preparation and characterization of cellulose microspheres. *Cellulose*, 18:135–142.

Thünemann, A., Klobes, P., Wieland, C., and Bruzzano, S. (2011). On the nanostructure of micrometer-sized cellulose beads. *Analytical and Bioanalytical Chemistry*, 401:1101–1108.

Trygg, J., Fardim, P., Gericke, M., Mäkilä, E., and Salonen, J. (2013). Physicochemical design of the morphology and ultrastructure of cellulose beads. *Carbohydrate Polymers*, 93:291–299.

Trygg, J., Fardim, P., Yildir, E., Kolakovic, R., and Sandler, N. (2014). Anionic cellulose beads for drug encapsulation and release. *Cellulose*, 21:1945–1955.

Vargaftik, N. B., Volkov, B. N., and Voljak, L. D. (1983). International tables of the surface tension of water. *Journal of Physical and Chemical Reference Data*, 12(3):817–820.

Vervaet, C., Baert, L., and Remon, J. P. (1995). Extrusion-spheronisation a literature review. *International Journal of Pharmaceutics*, 116(2):131–146.

Volkert, B., Wolf, B., Fischer, S., Li, N., and Lou, C. (2009). Application of modified bead cellulose as a carrier of active ingredients. *Macromolecular Symposia*, 280(1):130–135.

Weber, V., Linsberger, I., Ettenauer, M., Loth, F., Höyhtyä, M., and Falkenhagen, D. (2005). Development of specific adsorbents for human tumor necrosis factor-α: influence of antibody immobilization on performance and biocompatibility. *Biomacromolecules*, 6:1864–1870.

Weil, J., Sarikaya, A., Rau, S.-L., Goetz, J., Ladisch, C., Brewer, M., Hendrickson, R., and Ladisch, M. (1997). Pretreatment of yellow poplar sawdust by pressure cooking in water. *Applied Biochemistry and Biotechnology*, 68:21–40. 10.1007/BF02785978.

Weissenborn, P. K. and Pugh, R. J. (1996). Surface tension of aqueous solutions of electrolytes: Relationship with ion hydration, oxygen solubility, and bubble coalescence. *Journal of Colloid and Interface Science*, 184(2):550–563.

Westermarck, S. (2000). *Use of mercury porosimetry and nitrogen adsorption in characterisation of the pore structure of mannitol and microcrystalline cellulose powders, granules and tablets*. Academic dissertation, University of Helsinki.

Woodings, C. and Textile Institute (Manchester, England) (2001). *Regenerated Cellulose Fibres*. Woodhead Publishing Limited series on fibres. CRC Press, England.

Wu, J., Liang, S., Dai, H., Zhang, X., Yu, X., Cai, Y., Zhang, L., Wen, N., Jiang, B., and Xu, J. (2010). Structure and properties of cellulose/chitin blended hydrogel membranes fabricated via a solution pre-gelation technique. *Carbohydrate Polymers*, 79(3):677–684.

Xia, H.-F., Lin, D.-Q., Wang, L.-P., Chen, Z.-J., and Yao, S.-J. (2008). Preparation and evaluation of cellulose adsorbents for hydrophobic charge induction chromatography. *Industrial & Engineering Chemistry Research*, 47(23):9566–9572.

Xia, H.-F., Lin, D.-Q., and Yao, S.-J. (2007). Preparation and characterization of macroporous cellulose-tungsten carbide composite beads for expanded bed applications. *Journal of Chromatography A*, 1175(1):55–62.

Xiong, X., Zhang, L., and Wang, Y. (2005). Polymer fractionation using chromatographic column packed with novel regenerated cellulose beads modified with silane. *Journal of Chromatography A*, 1063:71–77.

Yang, B. and Wyman, C. E. (2006). BSA treatment to enhance enzymatic hydrolysis of cellulose in lignin containing substrates. *Biotechnology and Bioengineering*, 94(4):611–617.

Zhao, M., Li, J., Mano, E., Song, Z., Tschaen, D. M., Grabowski, E. J. J., and Reider, P. J. (1999). Oxidation of primary alcohols to carboxylic acids with sodium chlorite catalyzed by TEMPO and bleach. *The Journal of Organic Chemistry*, 64:2564–2566.

Zheng, H., Zhou, J., Du, Y., and Zhang, L. (2002). Cellulose/chitin films blended in NaOH/urea aqueous solution. *Journal of Applied Polymer Science*, 86(7):1679–1683.

Zogaj, X., Nimtz, M., Rohde, M., Bokranz, W., and Römling, U. (2001). The multicellular morphotypes of salmonella typhimurium and escherichia

coli produce cellulose as the second component of the extracellular matrix. *Molecular Microbiology*, 39(6):1452–1463.

Zugenmaier, P. (2001). Conformation and packing of various crystalline cellulose fibers. *Progress in Polymer Science*, 26(9):1341–1417.

6 Original research

Åbo Akademi University

FCT
ÅBO AKADEMI

BIOREGS

FIBIC
FINNISH BIOECONOMY CLUSTER

epnoe

Åbo Akademis förlag | ISBN 978-952-12-3168-1